

Modelling and Testing Aluminum Based High Entropy Alloys

A Major Qualifying Project Report
Submitted to the Faculty of
WORCESTER POLYTECHNIC INSTITUTE
in Partial Fulfillment of the Requirements for the
Degree of Bachelors of Science
in Mechanical Engineering
by

Arkady Governik _____

John G. Haddad _____

Connor M. Lemay _____

August 3, 2018

Approved by: _____

Professor Yu Zhong
Mechanical Engineering
WPI

Abstract

The purpose of this project was assist in the modeling, casting, and testing of aluminum based high entropy alloys. The goal was to create a castable alloy having more tensile strength than traditional aluminum alloys, while retaining properties such as being light weight and cost effective. This was done by modeling and casting alloys with FCC structures initially composed of aluminum, zinc, and magnesium, and later composed of aluminum, zinc, magnesium, copper, and silicon. This was done by conducting tensile test and castability experiments of the composed alloys to compare to other present alloys.

Acknowledgments

The project team would like to show our appreciation to the following people that helped make this project possible. A special thanks to the WPI Advanced Casting Research Center (ACRC) and Metal Processing Institute (MPI) for funding this project. A sincere thanks to Dr. Mohammad Asadikiya and Mr. Songge Yang for supporting us and guiding us in the right direction throughout the entirety of the project as well as assisting us by modelling each alloy for us. The project team would like to thank Michael Collins for teaching and assisting us with polishing, microscope analysis, and opening the door whenever we needed to get into the lab. Thanks to Dr. Libo Wang for guiding us through the casting process and showing us how to properly use the tensile testing machinery and composition tester. And of course, thank you to our advisor, Dr. Yu Zhong for keeping us on track and guiding us every step of the way.

Table of Contents

Abstract.....	1
Acknowledgments.....	2
Table of Contents.....	3
List of Figures.....	4
List of Tables.....	7
Introduction.....	8
Background.....	10
1. Cast One- 87.5% Al, 9.1% Zn, 3.4% Mg.....	16
1.1. Simulation.....	16
1.2. First Composition Test Results.....	18
1.3. Second Composition Test Results.....	20
1.4. Cast One Iteration 1.....	22
1.5. Cast One Iteration 2.....	29
1.6. Cast One Iteration 3.....	36
1.7. Final First Cast Conclusion.....	39
2. Cast Two- Hot Tearing.....	40
2.1. Introduction.....	40
2.2. 0% Silicon.....	46
2.3. 1% Silicon.....	48
2.4. 3% Silicon.....	50
2.5. Final Second Cast Conclusion.....	51
References.....	53
Appendix A: Modelling Process.....	55
Appendix B: Casting Process.....	56
Appendix C: Tensile Testing.....	60
Appendix D: Polishing Process.....	62
Appendix E: Optical Analysis Process.....	66

List of Figures

Figure 1: Molecular structures of various HEA's	10
Figure 2: Molecular structure BCC, FCC and HCP.....	11
Figure 3: The effects of Lattice Distortion increase as more elements are added to an alloy.....	12
Figure 4: CALPHAD ternary phase diagram	14
Figure 5: Ternary phase diagram of alloy at 250°C.....	15
Figure 6: Ternary phase diagram of alloy at 350°C.....	16
Figure 7: Ternary phase diagram of alloy at 450°C.....	16
Figure 8: Ternary phase diagram of alloy at 550°C.....	16
Figure 9: Phase diagram with secondary phases present.....	16
Figure 10: Graph of phase fraction based on temperature.....	17
Figure 11: Zoomed in view of 450°C phase diagram.....	17
Figure 12: Stress Strain Graph of 18.5 hr heat treated alloy	22
Figure 13: 50µm magnification at edge of 18.5 hr HT sample.....	23
Figure 14: 50µm magnification at center of 18.5 hr HT sample.....	23
Figure 15: Stress Strain Graph of 22 hr heat treated alloy.....	24
Figure 16: Metalography 50µm magnification at edge of 22 hr HT samples.....	24
Figure 17: Metalography 50µm magnification at center of 22 hr HT sample.....	24
Figure 18: Stress Strain Graph of 24 hr heat treated alloy	25
Figure 19: Stress Strain Graph of 24 hr heat treated alloy.....	26
Figure 20: Metalography 50µm magnification at edge of 24 hr HT sample.....	26
Figure 21: Metalography 50µm magnification at center of 24 hr HT sample.....	26
Figure 22: Stress Strain Graph of as cast.....	27
Figure 23: Metalography 50µm magnification at edge of as cast sample.....	27
Figure 24: Metalography 50µm magnification at center of as cast sample.....	27
Figure 25: Stress Strain Graph of 30 hr HT alloy.....	29
Figure 26: Stress Strain Graph of 30 hr HT alloy.....	30
Figure 27: Metalography 20µm magnification at edge of 30 hr HT sample.....	30
Figure 28: Metalography 20µm magnification at center of 30 hr HT sample.....	30

Figure 29: Stress Strain Graph of 8 hr aged sample.....	31
Figure 30: Stress Strain Graph of a second 8 hr aged sample.....	32
Figure 31: Metalography 20µm magnification at edge of 8 hr aged sample.....	32
Figure 32: Metalography 20µm magnification at center of 8 hr aged sample.....	32
Figure 33: Stress Strain Graph of the first 5 hr aged sample.....	33
Figure 34: Stress Strain Graph of a second 5 hr aged sample.....	34
Figure 35: Metalography 20µm magnification at center of 5 hr aged sample.....	34
Figure 36: Metalography 20µm magnification at center of 5 hr aged sample.....	34
Figure 37: Stress Strain Graph of as cast sample.....	35
Figure 38: Metalography 20µm magnification at edge of as cast sample.....	35
Figure 39: Metalography 20µm magnification at center of as cast sample.....	35
Figure 40: Stress Strain Graph of 30 hr HT.....	37
Figure 41: Stress Strain Graph of first 30 HT 5 hr aged sample.....	38
Figure 42: Stress Strain Graph of second 30 hr HT 5 hr aged sample.....	38
Figure 43: Comparison of first and third iteration samples.....	39
Figure 44: Cooling graph for cast 2.....	41
Figure 45: Picture of testing the cooling rate.....	41
Figure 46: Hot Tearing Sample for 0% Silicon.....	45
Figure 47: Hot Tearing Sample for 1% Silicon.....	48
Figure 48: Hot Tearing Sample for 3% silicon	50
Figure 49: Phase Diagram created using Thermo-Calc.....	55
Figure 50: Phase Diagram created using Pandat	55
Figure 51: Induction furnace control panel.....	57
Figure 52: Induction furnace with aluminum block.....	57
Figure 53: Adding metals to melted aluminum.....	57
Figure 54: Preparing sample for composition testing using belt sander.....	57
Figure 55: Composition testing sample	58
Figure 56: Bottom of sample after numerous composition testing.....	58
Figure 57: Melt being poured into castability mold.....	59
Figure 58: Cooled alloy in mold ready to be removed.....	59
Figure 59: Untested sample.....	60

Figure 60: Tensile testing machine Controls.....	60
Figure 61: Sample in tensile testing machine.....	61
Figure 62: Sample after testing.....	61
Figure 63: Buehler Metal Cutter used in project.....	63
Figure 64: Buehler Resin sample nounter used in project.....	64
Figure 65: Buehler Polisher used in project	65
Figure 66: Polished sample and carrying vessels.....	66
Figure 67: Nikon Microscope with sample being analysed.....	66

List of Tables

Table 1: Composition of alloy test piece.....	18
Table 2: Composition of alloy after adding zinc.....	20
Table 3: Hot Tearing rating table	43
Table 4: Composition of alloy before adding silicon.....	43
Table 5: Hot Tearing results for 1% silicon.....	47
Table 6: Composition for alloy contains 1% silicon.....	46
Table 7: Hot Tearing results for 1% silicon.....	47
Table 8: Composition of alloy containing 3% silicon.....	50
Table 9: Hot Tearing results for 3% silicon.....	51

Introduction

The study of material science has seen a substantial growth in the past 15 years due to new research on the field of High Entropy Alloys (HEAs). HEAs are materials which are generally composed out of at least 4-5 metals to create alloys with certain characteristics. Such characteristics may include high toughness, high melting point, lightweight, low cost, and high conductivity.[6]

The field of HEA has been investigated since the as early as the 1980's, but wide interest in the topic did not spark until the research publication of Jien-Wei Yeh followed by Brian Cantor who defined this field.[22] The reason for the recent growth in the field is the development of new computer modeling techniques that simulate the properties of a potential alloy before any experiments are done. This eliminates the need for a trial-and-error process which has potentially unlimited outcomes. Modeling is done by analysing the elements on an atomic level, taking into consideration how different elements bond and react with each other.[21]

The next step after creating a model of a future alloys is to cast the designed alloy, test its mechanical properties and observe its structure. Manufacturing HEAs can be done by using different methods, including arc melting, Bridgman Solidification, and manufacturing from powder. During arc melting, the torch temperature in the furnace is approximately 3000C, and is controlled by adjusting the electrical power. This method is not suitable for low melting elements such as Magnesium, Zinc or Manganese because they can easily evaporate. In these cases induction heating is a more adequate method. The Bridgman solidification or the Bridgman-Stockbarger method is a technique used to grow single crystal ingots. In this method, the material is heated above its melting point and then slowly cooled down from the one end of its container, where a seed crystal is located. A single crystal of the same crystallographic orientation as the seed material is grown on the seed, and progressively formed along the length of the container. The Bridgman method is used to produce certain semiconductor crystals and can be carried out in a horizontal or vertical geometry. There are several methods to manufacture an alloy from powder, one of them is done by a concentrated laser beam that melts the synchronously fed powders and a thin layer of the substrate. The metallic powders undergo a

rapid melting and cooling process. Meanwhile, a metallurgical bonding can be formed between the substrate and the powders.[2]

After substantial research, materials scientists learned that aluminum in specific has several properties that can be beneficial valuable to HEAs. Aluminum is known to form Gamma particles that enhance strength and creep resistance, it also forms a protective oxide scale which improves oxidation and corrosion resistance. Furthermore, aluminum is the most effective element in preventing austenite grain growth in case steel is a component of the alloy, and aluminum often significantly reduces the density of the alloy.[12]

This report will focuses on the casting process and testing of aluminum based HEAs while modeling the modelling part will be done by a research team from the WPI Advanced Casting Research Center (ACRC).

Background

High Entropy Alloys

There is currently no standard definition of HEAs, but it is widely accepted that alloys consisting of at least five elements, each at 5-35% of the alloy by composition, are considered to be HEAs [1]. The presence of multiple principal elements in an alloy results in high configurational entropy compared to traditional alloys [2]. Controlling the configurational entropy of an alloy could be used to stabilize solid solution phases in order to achieve and improve a material's specific mechanical and thermodynamic properties [1].

Tests conducted on HEAs have found that the properties of HEA's are superior to those of conventional alloys. Researchers at North Carolina State University have been able to create a HEA with a higher strength-to-weight ratio than any other existing alloy [3]. HEAs have produced significant increases in mechanical and thermodynamic properties, such as ductility, fracture resistance, and conductivity, compared to traditional alloys [4].

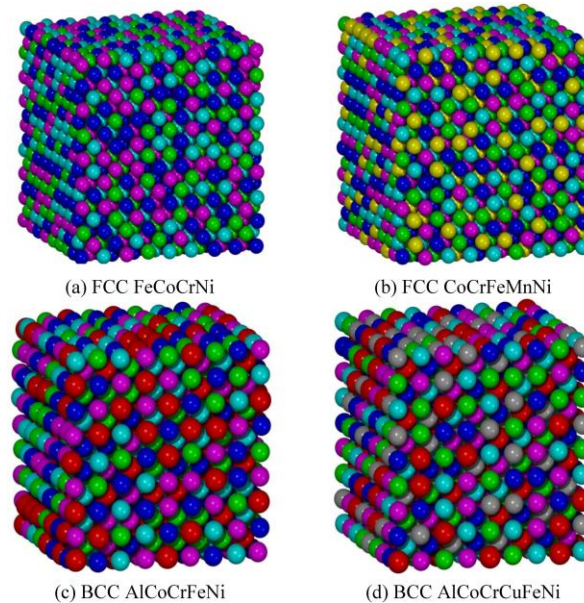


Figure 1. Molecular structure of various HEA [5]

The superior mechanical and thermodynamic properties of HEAs result from the interactions between the different elements in the alloy. These interactions produce what is referred as the “Core Effects”. There are four “Core Effects” that exist in HEAs; the “High Entropy Effect”, the “Sluggish Diffusion Effect”, the “Severe Lattice Distortion Effect”, and the “Cocktail Effect” [2].

The “High Entropy Effect” is the foundation of HEAs. It states that high levels of entropy can stabilize a disordered solid solution phase [2]. Prior to the recent testing and research conducted on HEA’s, it was believed that alloys that contained multiple principle elements would be unstable and brittle [2]. Recent research, however, shows that because the elements in HEAs exist in more equal proportions, the interactions between the elements tend to result in single phase solid solution microstructures with FCC, BCC and HCP crystal structures [6].

FCC (face centered cubic), BCC (body centered cubic) and HCP (hexagonal close packed) are the most commonly found crystal structures [7]. In the cubic structure of BCC crystals, there is one atom at the center of the cube and one atom at each of the cube’s eight corners [7]. In the cubic structure of FCC crystals, there is one atom at each of the cube’s eight corners and one atom at each of the cube’s six faces [8]. The hexagonal structure of HCP consists of alternating stacked layers of atoms arranged in a hexagonal pattern [7]. The structures of BCC, FCC and HCP are shown in figure 2 for more clarity.

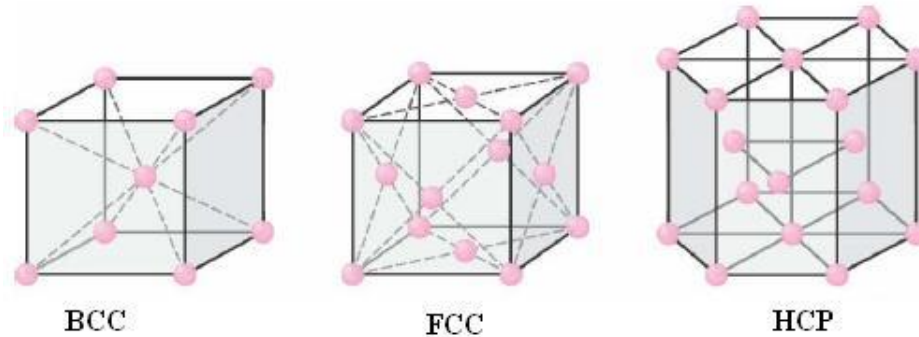


Figure 2. Molecular structures of BCC, FCC and HCP [9]

The “High Entropy Effect” exists because of what is known as Gibbs Free Energy. Gibbs Free Energy (G) is the thermodynamic potential of a system at constant pressure and temperature [10]. Gibbs Free Energy is calculated with the equations $G=H-T\cdot S$ and $\Delta G_{\text{mix}} = \Delta H_{\text{mix}}-T\cdot \Delta S_{\text{mix}}$, where H is enthalpy, T is absolute temperature, S is entropy, ΔG_{mix} is Gibbs Free Energy of mixing, ΔH_{mix} is enthalpy of mixing, and ΔS_{mix} is entropy of mixing [10]. A phase becomes more stable as G decreases and becomes a single solid solution if ΔG_{mix} is negative [2]. Based off of the equations above, Gibbs Free Energy will decrease as entropy increases, therefore creating a stable single solid solution.

The “Sluggish Diffusion Effect” states that kinematic transformations occur more slowly in HEAs than in conventional alloys because of the higher activation energies and atomistic

phenomena of HEAs [2]. Slower kinematic transformations are the reason why HEAs have higher fracture resistance, hardness and thermodynamic properties compared to conventional alloys.

The “Severe Lattice Distortion Effect” states that the crystalline structures of HEAs are actually deformed [2]. This distortion is created by the differences in size and bonding energy of the different elements, and causes both compression and tension within the lattice. This strengthens the stress-strain field and increases the energy of the lattice [10].

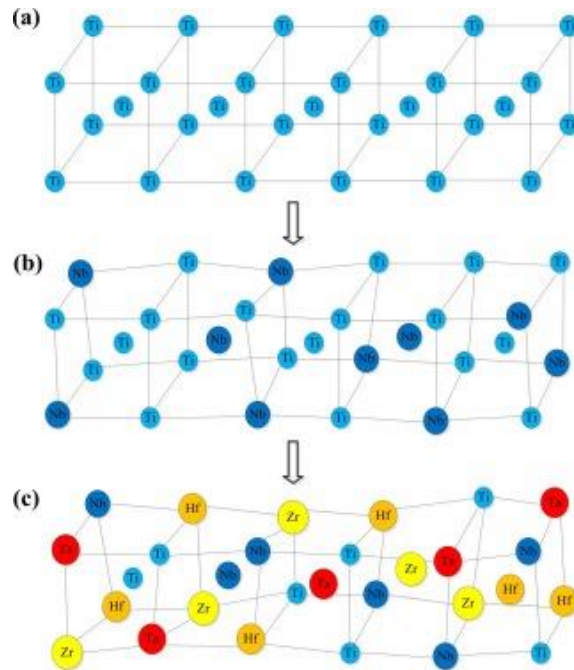


Figure 3. The effects of Lattice Distortion increase as more elements are added to an alloy. [11]

The last of the “Core Effects” is the “Cocktail Effect”, which states that the strength of a HEA is much higher than the average strength of the elements in its composition [2]. Interactions between different elements create forces in HEAs which are not present in conventional alloys. These forces allow for HEAs to be stronger than the average strength of the elements in its composition.

HEAs have many applications. Due to their high strength-to-weight ratios, they have practical applications in industries in which materials must be both lightweight and strong, such as the aerospace and automotive industries. HEAs exhibit superior thermodynamic properties, and can be used under very high temperatures.

Aluminum Based Alloys

Aluminum is one of the most commonly used metals in manufacturing. Aluminum and aluminum based alloys are commonly used due to their low densities, low cost, oxidation resistance, and electrical and thermal properties [12]. While the benefits of aluminum in conventional alloys are widely understood, it is still unclear exactly how much aluminum improves HEAs [4]. One known benefit of aluminum based HEA's is that they commonly have FCC structures [6]. The atoms in FCC structures are more tightly packed and therefore create a harder and stronger structure than BCC and other structures [7].

Modeling Process

ICME (Integrated Computational Materials Engineering) are computer programs that create simulations and models of materials [13]. ICME's allow manufacturers to create materials more efficiently and at a lower cost because they can model and test the material without having to actually create the material. Of all the ICME programs, CALPHAD is arguably the most advanced. **CAL**culat**ion** of **PH**ase **D**iagrams is an ICME program that calculates the phases of materials and creates phase diagrams [14]. CALPHAD models the Gibbs Free Energy for each phase of a material and then calculates the phase or combination of phases which has the lowest amount of Gibbs Free Energy, and is therefore the most stable [2]. CALPHAD can be used to create phase diagrams using many variables, such as the percentage of each component and temperature, and can use both ternary and binary diagrams [14]

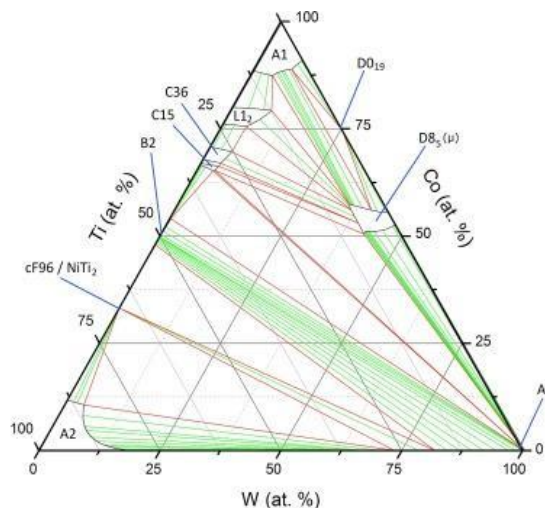


Figure 4. CALPHAD ternary phase diagram [15]

Metallography

Metallography is the study of metallic alloys and their microstructures to determine their phases and properties [16]. Metallography typically involves polishing and resin molding samples of an alloy to view its structure under a high power microscope. This allows researchers to determine the phases and structural defects of a material to better understand the material's properties, and to better understand the results of mechanical testing.

Cast One: 87.5% Al, 9.1% Zn, 3.4% Mg

1.1. Simulation

Procedural Overview

ICME modeling programs are used to simulate materials and calculate their phases before casting the actual material. The two CALPHAD programs used in this project were Pandat and Thermo-Calc. These programs were used to create an aluminum based alloy with a pure FCC structure.

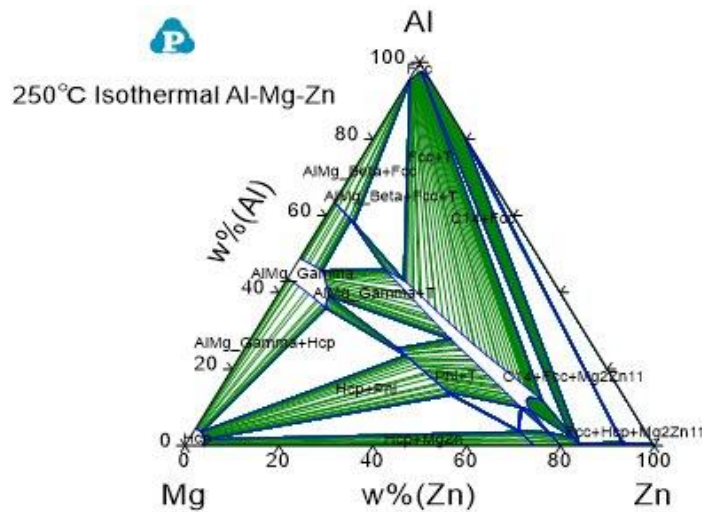


Figure 5: Ternary Phase of alloy at 250°C

The first stage of this process was to find what elements, when mixed with aluminum, produced FCC phases. Once these elements were determined, we calculated which combinations produced pure FCC, and determined the combination with the largest amount of pure FCC. Pandat and Thermo-Calc were then used to determine what heat treatment temperature and composition would produce the largest amount of FCC.

Results

While many of the aluminum based binary alloys produced pure FCC phases, a promising high entropy candidate included a mixture of aluminum, zinc, and magnesium. This combination was the only one with a large enough, if any, pure FCC region. The following ternary graphs were created to determine the heat treatment and composition of the alloy.

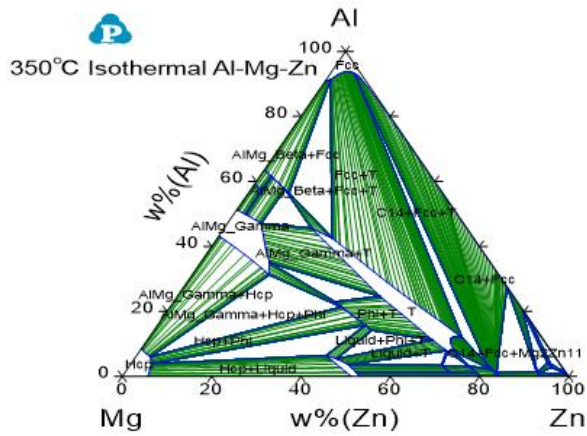


Figure 6 (Left): Ternary Diagram of alloy at 350°C

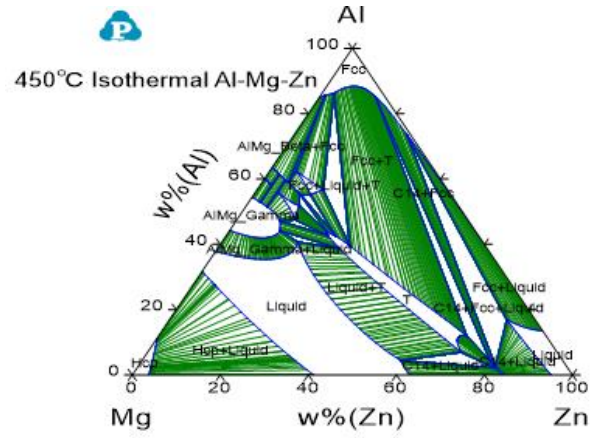


Figure 7(Right): Ternary Diagram of alloy at 450°C

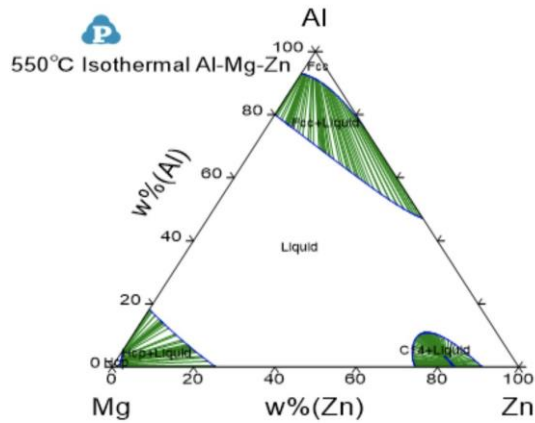


Figure 8 (Left): Ternary Diagram of alloy at 550°C

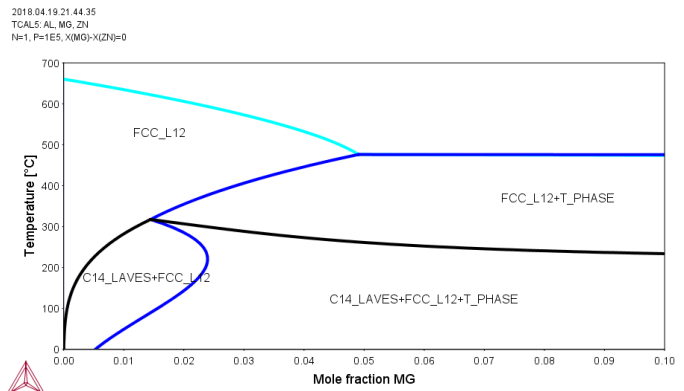


Figure 9 (Right): Phase diagram of alloy with secondary phase present

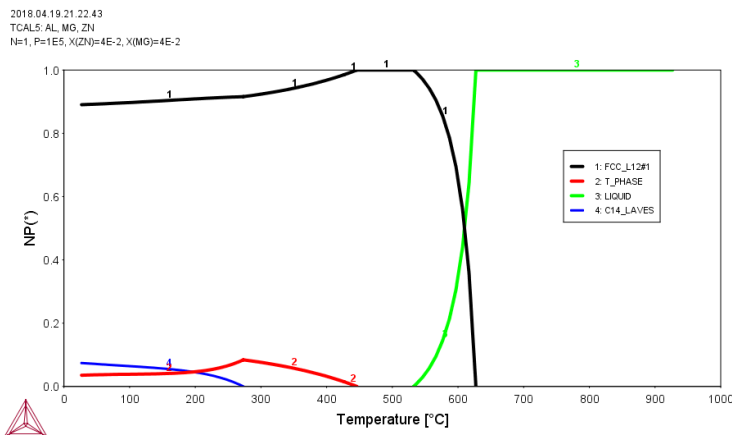


Figure 10: Graph of phase fraction based on temperature

Conclusion

Based on the data presented above, the selected heat treatment was 470°C, with 480°C and 460°C also tested throughout the project. The following weight percent composition of 87.5% Aluminum, 9.1% Zinc and 3.4% Magnesium was selected. Aging temperatures included 200°C, 300°C, and 120°C based upon the phase diagram produced and test results.

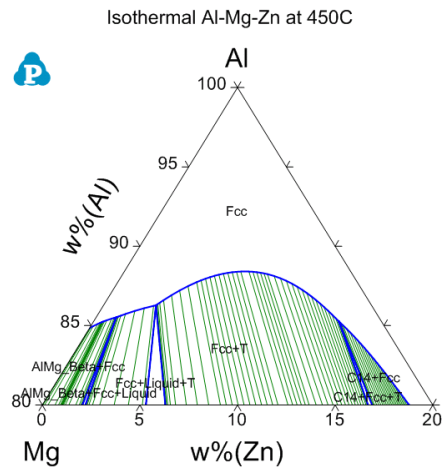


Figure 11: Zoomed in view of 450°C Ternary Diagram

1.2. First Composition Test Results

Table 1: Composition of alloy test piece

No	Si	Fe	Cu	Mn	Mg	Cr	Ni	Zn
	%	%	%	%	%	%	%	%
1	0.0018	0.0081	0.0014	<0.0003	3.42	0.001	0.0004	8.99
2	<0.0005	0.0072	0.0013	<0.0003	3.42	0.001	0.0004	9
3	<0.0005	0.0071	0.0013	<0.0003	3.47	0.001	0.0004	9.08
4	<0.0005	0.0057	0.0011	<0.0003	3.44	0.001	0.0004	9.03
5	<0.0005	0.0075	0.0013	<0.0003	3.49	0.001	0.0004	9.13
x	0.0005	0.0071	0.0013	<0.0003	3.45	0.001	0.0004	9.05
No	Ti	Ag	B	Ba	Be	Bi	Ca	Cd
	%	%	%	%	%	%	%	%
1	0.0004	0.0024	0.0006	<0.0001	0.0006	<0.001	0.0007	0.0001
2	0.0004	0.0024	0.0005	<0.0001	0.0006	<0.001	0.0013	0.0003
3	0.0004	0.0024	0.0006	<0.0001	0.0006	<0.001	0.0005	0.0003
4	0.0004	0.0024	0.0005	<0.0001	0.0006	<0.001	0.0004	0.0001
5	0.0004	0.0024	0.0005	<0.0001	0.0006	<0.001	0.0012	0.0001
x	0.0004	0.0024	0.0005	<0.0001	0.0006	<0.001	0.0008	0.0001

No	Ce	Co	Ga	In	Li	Na	P	Pb
	%	%	%	%	%	%	%	%
1	<0.0015	<0.0005	<0.001	0.0003	0.0001	0.0003	0.0023	0.0005
2	<0.0015	<0.0005	<0.001	0.0003	0.0001	0.0005	0.0021	0.0005
3	<0.0015	<0.0005	<0.001	0.0003	0.0001	0.0001	0.0022	0.0005
4	<0.0015	<0.0005	<0.001	0.0003	0.0001	0.0002	0.002	0.0005
5	<0.0015	<0.0005	<0.001	0.0003	0.0001	0.0005	0.002	0.0005
x	<0.0015	<0.0005	<0.001	0.003	0.0001	0.0003	0.0021	0.0005
No	Sb	Sn	Sr	V	Zr	Hg	Al	
	%	%	%	%	%	%	%	
1	0.002	0.001	0.0001	0.0006	0.0003	0.002	87.6	
2	0.002	0.001	0.0001	0.0007	0.0003	0.002	87.6	
3	0.002	0.001	0.0001	0.0005	0.0003	0.002	87.4	
4	0.002	0.001	0.0001	0.0006	0.0003	0.002	87.5	
5	0.002	0.001	0.0001	0.0005	0.0003	0.002	87.4	
x	0.002	0.001	0.0001	0.0006	0.0003	0.002	87.5	

The desired composition of our cast was 87.5% Al, 9.1% Zn and 3.4% Mg.

The first composition test results show that our mold consisted of 87.5% Aluminum, 3.45% Magnesium and 9.05% Zinc. From this we determined adding more zinc would get the composition closer to what we required.

1.3. Second Composition Test Results

Table 2: Composition of alloy after adding zinc

No	Si	Fe	Cu	Mn	Mg	Cr	Ni	Zn
	%	%	%	%	%	%	%	%
1	<0.0005	0.035	0.00012	0.0003	3.38	0.0013	0.0004	9.11
2	<0.0005	0.033	0.0012	0.0003	3.41	0.0013	0.0004	9.21
3	<0.0005	0.017	0.0013	0.0003	3.36	0.0011	0.0004	9.08
4	<0.0005	0.015	0.001	0.0003	3.32	0.0012	0.0004	9.03
5	<0.0005	0.013	0.0011	0.0003	3.32	0.0011	0.0004	8.99
6	<0.0005	0.012	0.0011	0.0003	3.39	0.0011	0.0004	9.15
x	<0.0005	0.021	0.0012	0.0003	3.36	0.0012	0.0004	9.09
No	Ti	Ag	B	Ba	Be	Bi	Ca	Cd
	%	%	%	%	%	%	%	%
1	<0.0004	0.0024	0.0006	<0.0001	0.0006	<0.001	0.0008	0.0002
2	<0.0004	0.0024	0.002	<0.0001	0.0006	<0.001	0.0028	0.0001

3	<0.0004	0.0023	0.0007	<0.0001	0.0006	<0.001	0.0017	0.0004
4	<0.0004	0.0023	0.0007	<0.0001	0.0006	<0.001	0.0013	0.0002
5	<0.0004	0.0022	0.0006	<0.0001	0.0006	<0.001	0.0016	0.0006
6	<0.0004	0.0024	0.0009	<0.0001	0.0006	<0.001	0.0016	0.0004
x	<0.0004	0.0023	0.0009	<0.0001	0.0006	<0.002	0.0016	0.0003

No	Ce	Co	Ga	In	Li	Na	P	Pb
	%	%	%	%	%	%	%	%
1	<0.0015	<0.0005	<0.001	0.0003	0.0001	0.0007	0.0021	0.0005
2	<0.0015	<0.0005	<0.001	0.0003	0.0001	0.0006	0.0021	0.0005
3	<0.0015	<0.0005	<0.001	0.0003	0.0001	0.0014	0.0018	0.0005
4	<0.0015	<0.0005	<0.001	0.0003	0.0001	0.0006	0.0022	0.0005
5	<0.0015	<0.0005	<0.001	0.0003	0.0001	0.0012	0.0022	0.0005
6	<0.0015	<0.0005	<0.001	0.0003	0.0001	0.0004	0.0018	0.0005
x	<0.0015	<0.0005	<0.001	0.0003	0.0001	0.0008	0.002	0.0005
No	Sb	Sn	Sr	V	Zr	Hg	Al	
	%	%	%	%	%	%	%	
1	0.002	0.001	0.0001	0.0006	0.0003	0.002	87.5	

2	0.002	0.001	0.0001	0.0005	0.0003	0.002	87.3
3	0.002	0.001	0.0001	0.0007	0.0014	0.002	87.5
4	0.002	0.001	0.0001	0.0005	0.0003	0.002	87.6
5	0.002	0.001	0.0001	0.0005	0.0003	0.002	87.7
6	0.002	0.001	0.0001	0.0005	0.0003	0.002	87.4
x	0.002	0.001	0.0001	0.0005	0.0003	0.002	87.5

1.4. Cast 1 Iteration 1

From theoretical knowledge, it was estimated that a cast such as our will require a minimum of 18 hours of heat treatment in order for proper Face-Centred Cubic phase transformation. To find the ideal time of heat treatment, we tested several of the casted tensile bars under different lengths of heat treatment at 470°C. Thus, we chose heat treatment lengths of 0, 18.5, 22, 24 hours. This iteration involved five sample pieces. One as-cast, one heat treated for 18.5 hours, one heat treated for 22 hours, and two heat treated for 24 hours. After each sample completed the desired heat treatment time each sample was air quenched, meaning it was cooled solely by being left out in the room until the temperature decreased.

18.5 Hour Heat Treatment

Tensile Test Results

Load at break: 8470.922 lbf

Young's Modulus: 9551.079 ksi

Tensile stress at break: 41.467 ksi

Strain % at break: 0.501

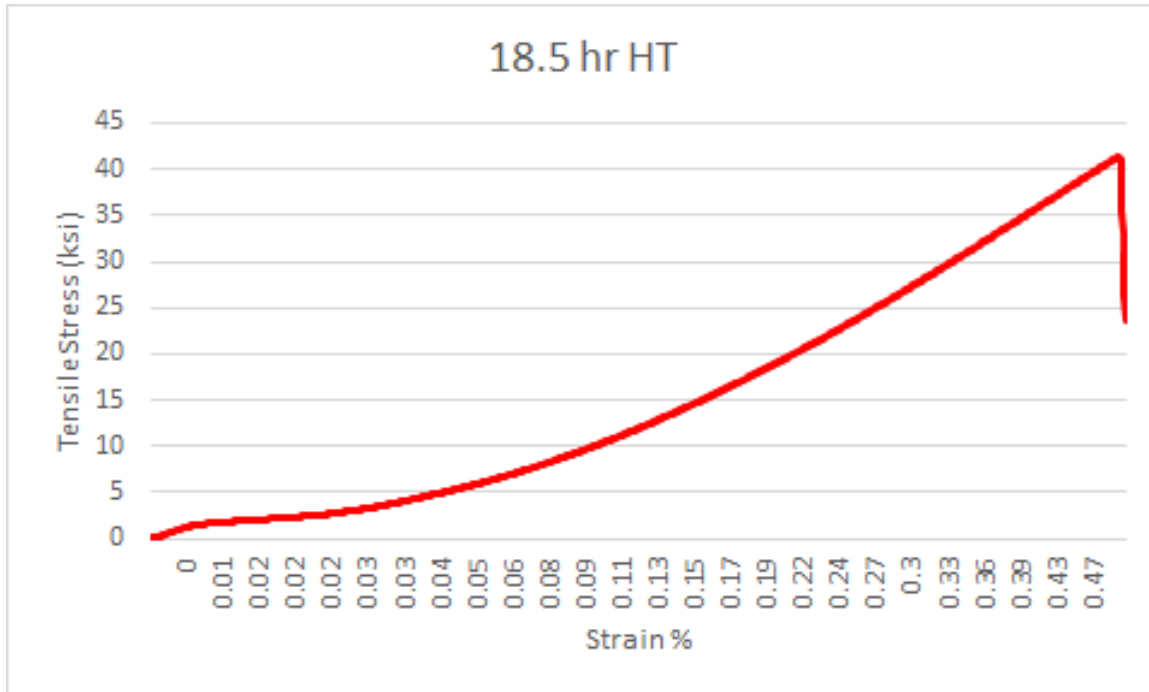


Figure 12: Stress strain graph of 18.5 hr heat treated alloy

Optical images

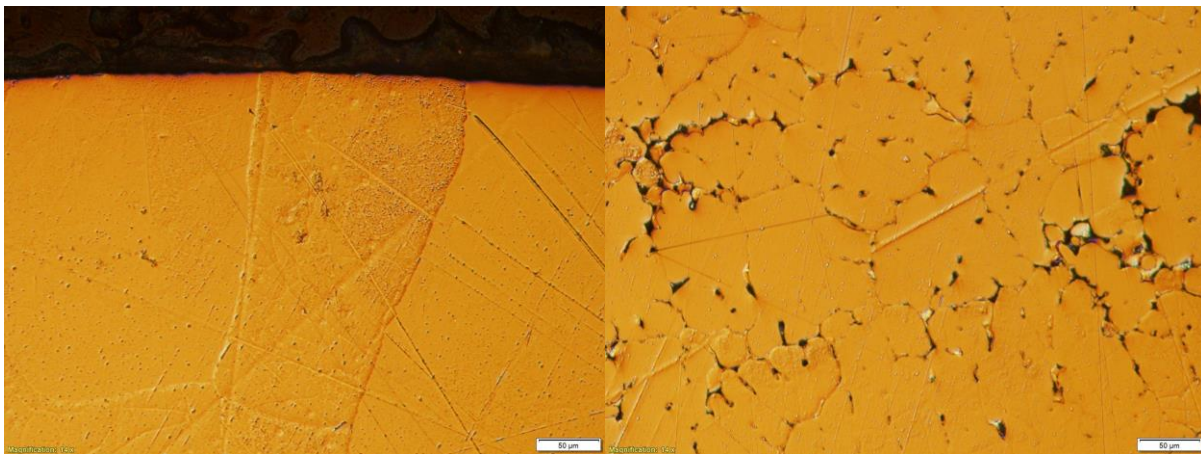


Figure 13 (Left): 50μm magnification at edge of 18.5hr HT sample

Figure 14(Right): 50μm magnification at center of 18.5 hr HT sample

Analysis of sample

The sample experienced brittle fracture when being tested for material properties within the desired break region. When observed under a microscope after polishing, there were sparse amounts of secondary phase precipitates around the edge of the sample but there was black shading in the middle of the sample that can be either secondary phase or pores, observation under the SEM is needed to draw a final conclusion.

22 Hour Heat Treatment

Tensile Test Result

Load at break: 9592.607 lbf

Young's Modulus: 11283.267 ksi

Tensile stress at break: 46.958 ksi

Strain % at break: 0.564

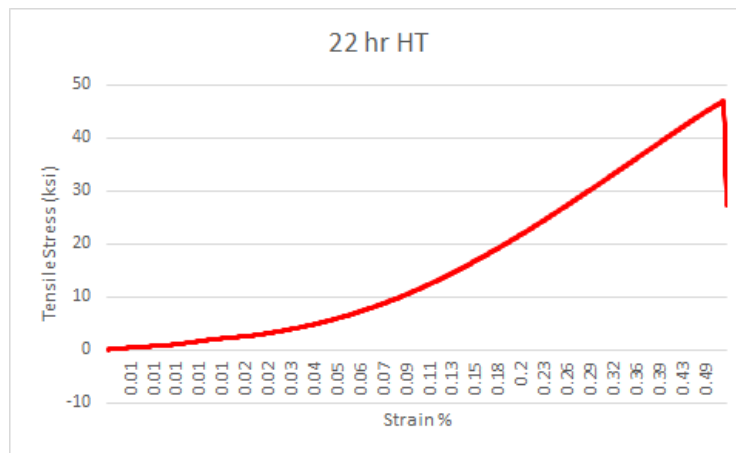


Figure 15: Stress strain graph of 22 hr heat treated alloy

Optical Images

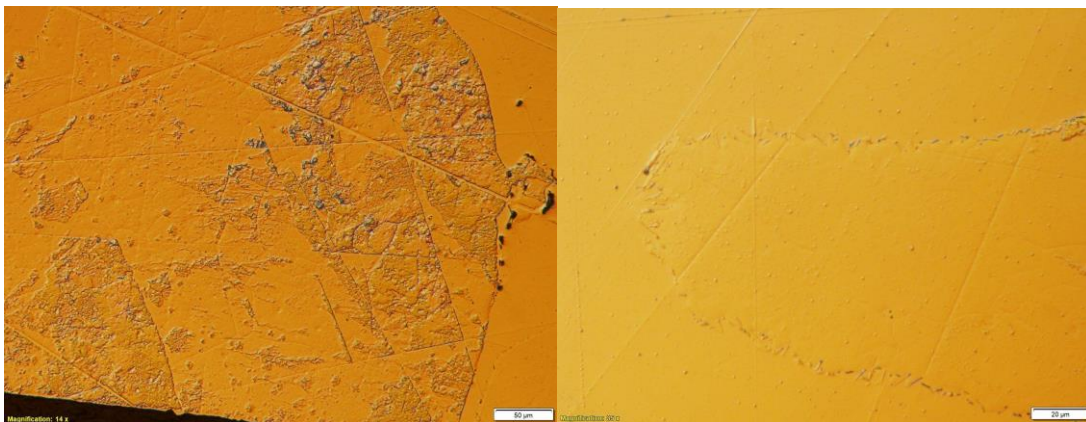


Figure 16 (Left): 50µm magnification at edge of 22 hr HT sample

Figure 17 (Right) 50µm magnification at center of 22 hr HT sample

Analysis of sample

The sample experienced brittle fracture within the desired break region when being mechanically tested. When observed under the microscope after polishing there was more formation of precipitates along the edge than the 18.5 hour and the density of the precipitates remained even throughout the sample, both edge and center.

24 Hour Heat Treatment

Sample One:

Tensile Test Result

Load at break: 9277.419 lbf

Young's Modulus: 10140.850 ksi

Tensile stress at break: 45.415 ksi

Strain % at break: 0.513

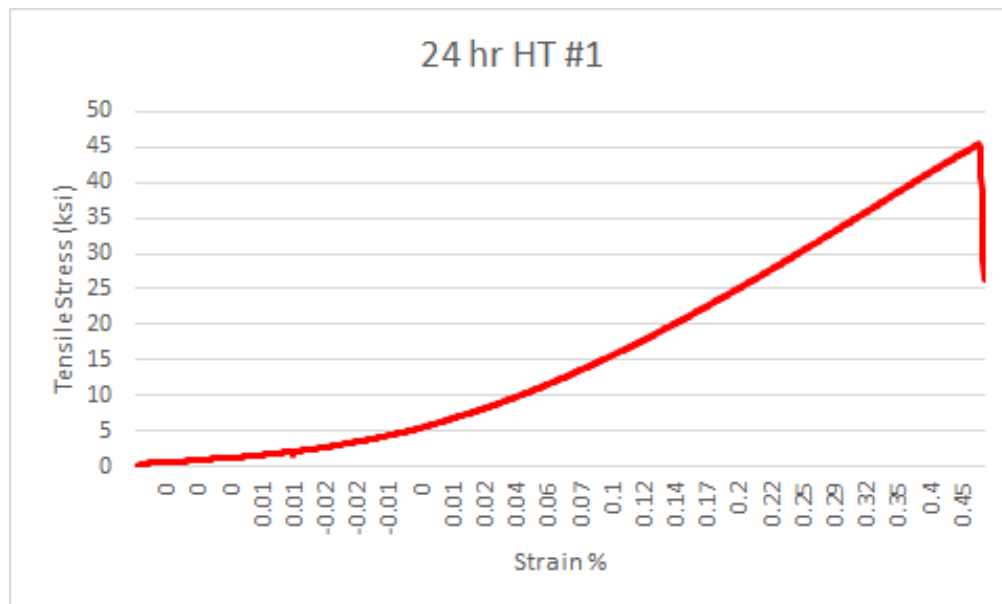


Figure 18: Stress strain graph of one of two 24 hr heat treated pieces

Sample Two:

Tensile Test Result

Load at break: 9318.026 lbf

Young's Modulus: 10370.557 ksi

Tensile stress at break: 45.614 ksi

Strain % at break: 0.645

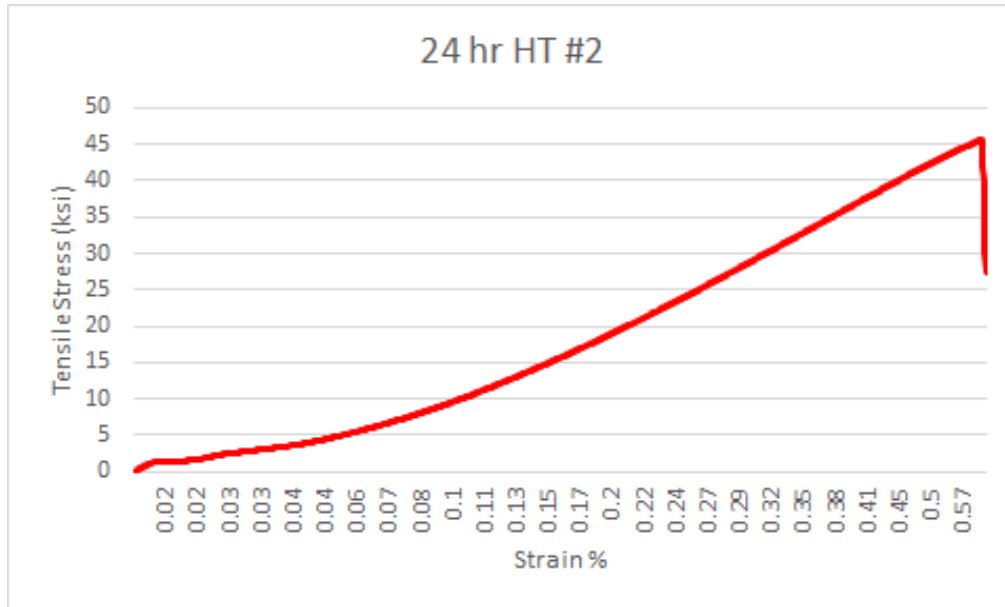


Figure 19: Stress strain graph of second 24 hr heat treated sample

Optical Images

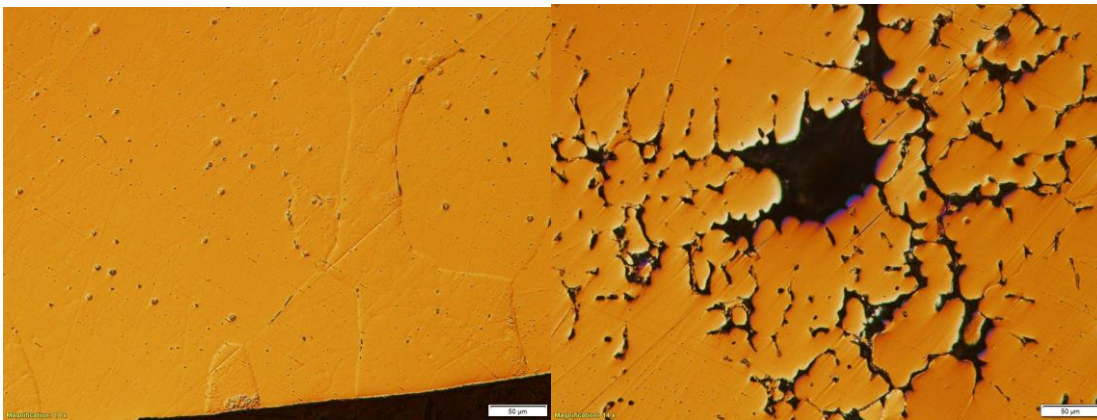


Figure 20 (Left) 50μm magnification at edge of 24 hr HT sample

Figure 21 (Right) 50μm magnification at center of 24 hr HT sample

Analysis of samples

Both samples experienced brittle fracture within the desired breakage region when being mechanically tested. When observed under a microscope, the edge had precipitate present, but the middle had heavy amounts of secondary phase creating a porous alloy.

As-Cast

Tensile Test Result

Load at break: 8387.536 lbf

Young's Modulus: 10472.040 ksi

Tensile stress at break: 41.0586 ksi

Strain % at break: 0.550

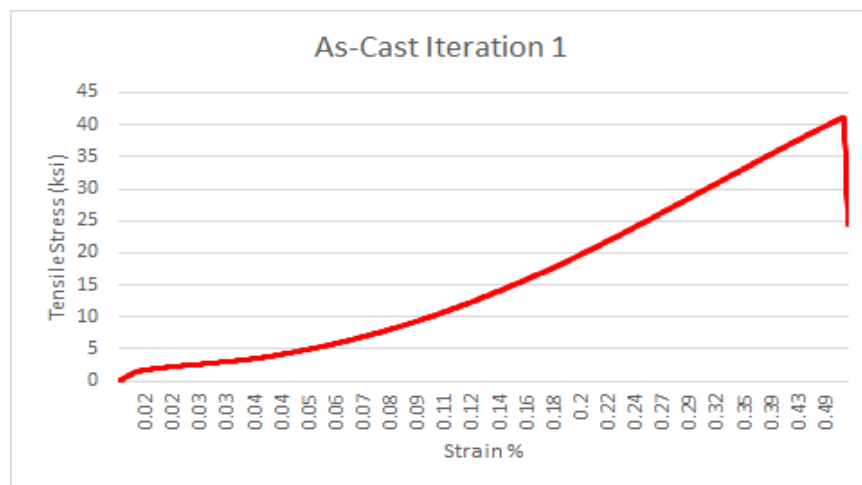


Figure 22: Stress strain graph of as-cast

Optical Images



Figure 23 (Left): 50µm magnification at edge of as cast sample

Figure 24 (Right): 50µm magnification at center of as cast sample

Analysis of sample

The as-cast experienced brittle fracture when being mechanically tested. When observed after polishing, there were bubbles of precipitate evenly spread throughout the sample.

First Tensile Testing Analysis of Results

From these few tests, we can see that our alloy has higher tensile strength than pure aluminum, but is less ductile. When analyzing the point of fracture, we saw that the alloy has brittle characteristics such as dendrites on the fracture surface. Heat treating did add more ductility to the alloys but was not consistent through all sample

Analysis of Sample Under Microscope

At the edge of the sample:

The more the sample was heat treated, present precipitates became smaller, but remained evenly distributed. All edges had formation of precipitates at the grain boundaries, but were small compared to grain boundary formation in the central region.

At the center region of sample:

Heavy precipitate formation along grain boundaries, most spanning along the whole edge of visible grain. This was only visible with two samples, 18.5 hr and 24 hr heat treatment. When analyzing the other two samples, precipitates were present within the grains and were more frequent than at the edge. The size of the precipitates in 22 hours of heat treatment were noticeably smaller than in the as-cast sample.

Cast One Iteration One Conclusion

By looking at the structure of the samples under a microscope and the tensile tests results, it is clear that heat treatment helped creating a more defined structure in the alloy. Heat treatment would not be advised to go over 24 hours due to production factors.

For future testing of the next iterations, more samples should be tested under various heat treatment times and quenching methods in order to find a general mean performance of the alloys. We can also conduct these experiments under heat in order to observe the characteristics of the alloys at high temperatures.

The samples were taken to the Scanning Electron Microscope (SEM) for further analysis of precipitations within the grain and at the grain boundary. Composition of these precipitates were determined through this method.

1.5. Cast 1 Iteration 2

For our second iteration of our initial cast, we specifically looked at the phase diagram chart for the produced alloy (figure E). From this we devised a plan to heat treat and age certain samples to achieve each phase shown in the diagram. This iteration involved 7 sample pieces, two going into each phase with one more as-cast to use as a baseline. Each went through a specific heat treatment and aging regimen followed by the use of water quenching instead of air quenching used in the first iteration. The results are as follows:

Pure Face Centered Cubic (FCC) (2 pieces)

The first two pieces were heat treated and aged to achieve a pure FCC crystal structure. This required the sample pieces to undergo heat treatment at 480°C for 30 hours. They were then immediately quenched in water and brought to tensile testing so no aging could occur.

Tensile Testing Results

Sample Piece One:

Load at break: 9035.33 lbf

Young's Modulus: 11243.976 ksi

Tensile Stress at break: 44.229 ksi

Strain % at break: 0.109

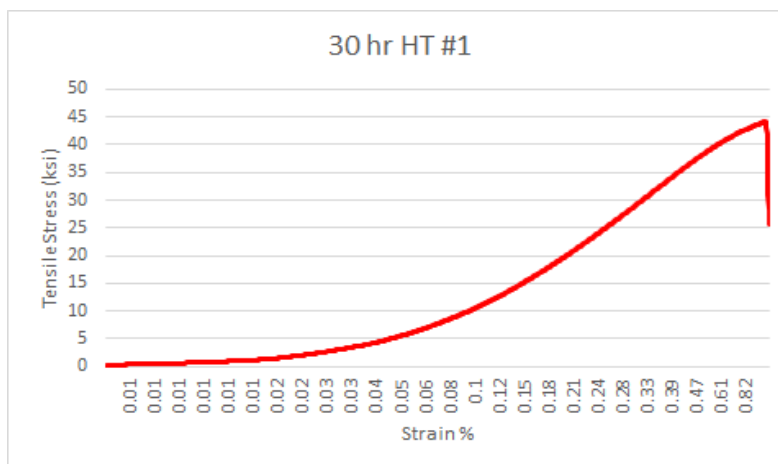


Figure 25: Stress strain graph of 30 hr heat treated alloy

Sample Piece Two:

Load at break: 7492.901 lbf

Young's Modulus: 10165274 psi

Tensile Stress at break: 36.679 ksi

Strain % at break: 0.115

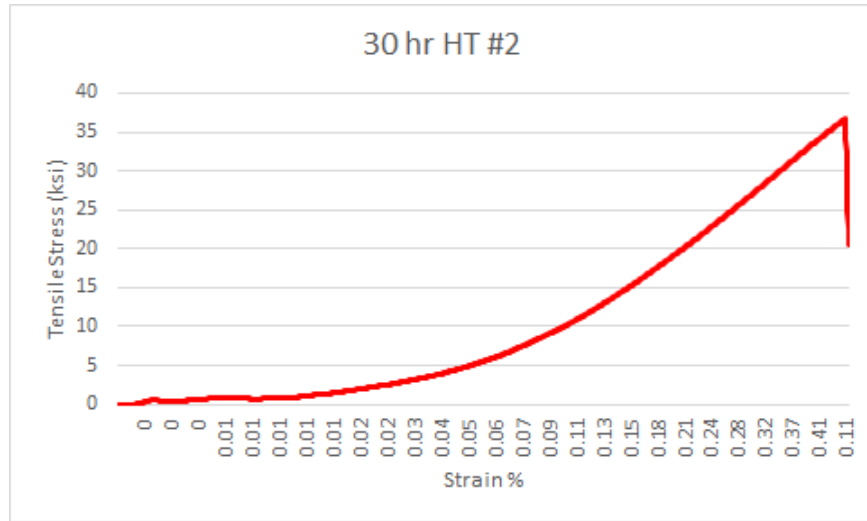


Figure 26: Stress strain graph of second 30 hr heat treated alloy

Optical images

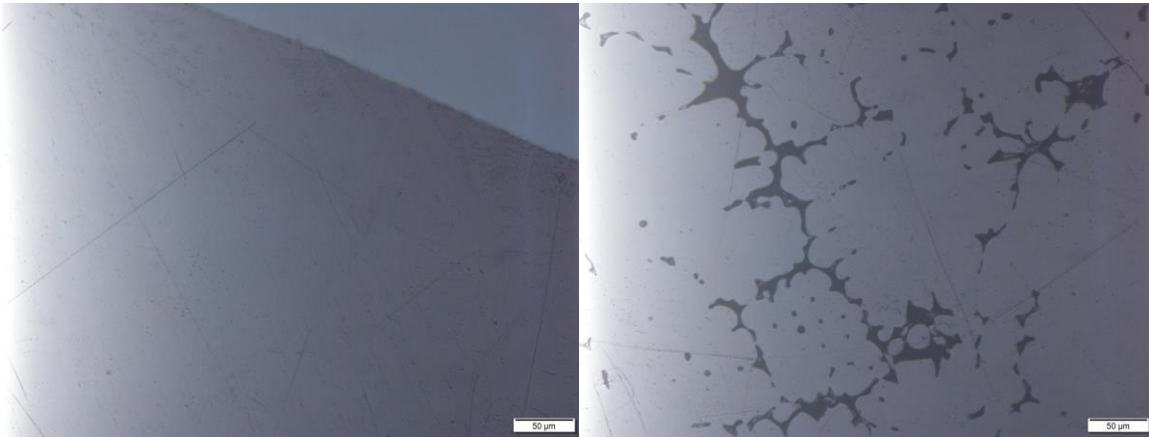


Figure 27 (Left): 20µm magnification at edge of 30 hr HT sample

Figure 28 (Right): 20µm magnification at center of 30 hr HT sample

Analysis of samples

Samples experienced brittle fracture within the testing range when being mechanically tested. When observed under the microscope, the edges had no sign of precipitation or secondary phases. In the middle of the sample there were large deposits of secondary phase, leaving the samples porous.

FCC + T-Phase (2 pieces)

The next two pieces were treated and aged to achieve a FCC crystal structure with a secondary T phase to be present in grain boundaries. To do this, we heat treated the samples for 30 hours at 480°C and immediately water quenched them. We then aged the samples in a 200°C oven for 8 hours, water quenching the samples immediately after.

Tensile Testing Results

Sample Piece Three:

Load at break: 6185.30 lbf

Young's Modulus: 10482.959 ksi

Tensile Stress at break: 30.278 ksi

Strain % at break: 0.342

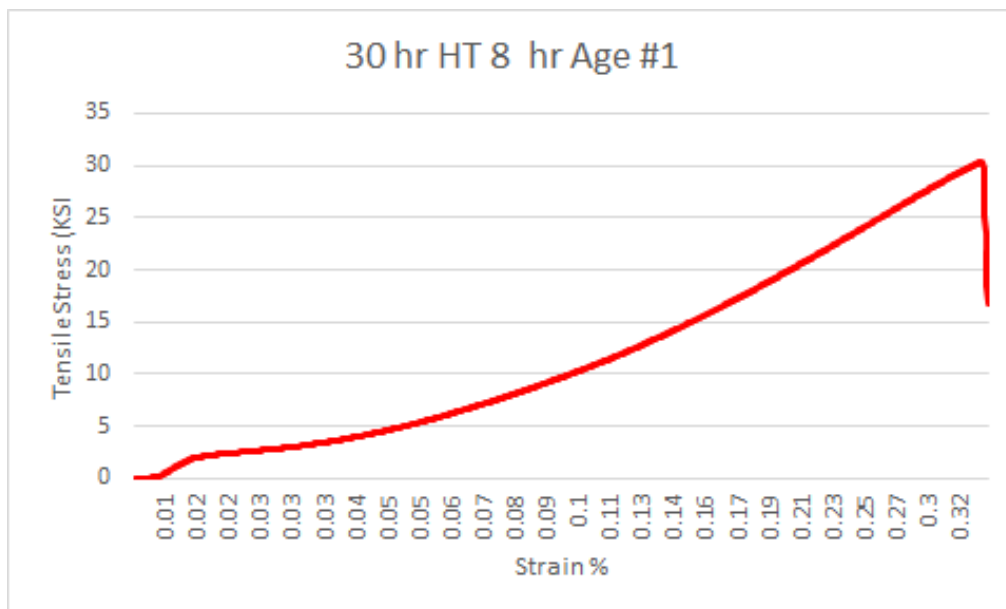


Figure 29: Stress strain graph of 8 hr aged sample

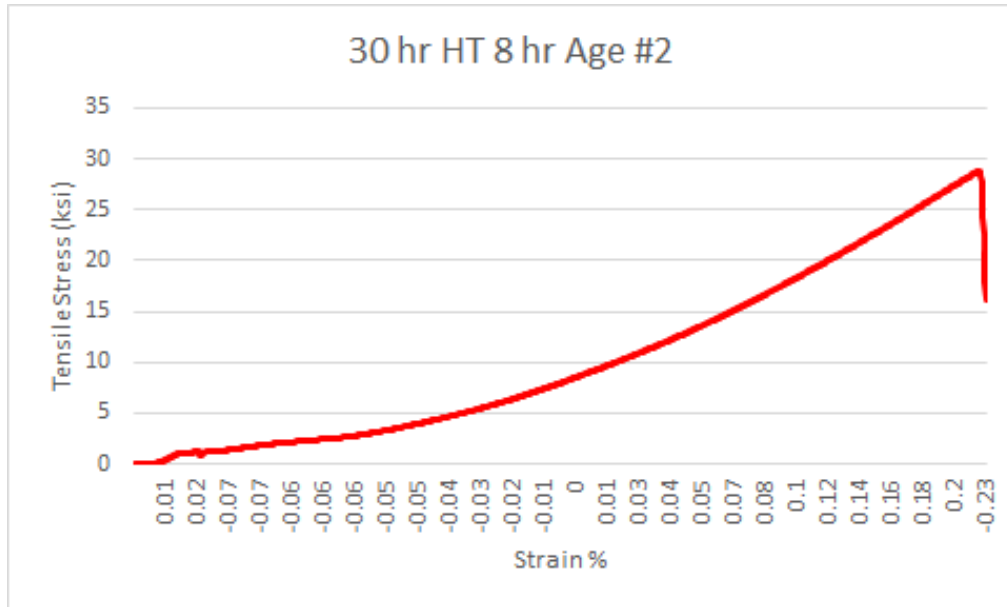
Sample Piece Four:

Load at break: 5899.847 lbf

Young's Modulus: 9669.455 ksi

Tensile stress at break: 28.881 ksi

Strain % at break: 0.226



Forgive 30: Stress strain graph of a second 8 hr aged sample

Optical Images

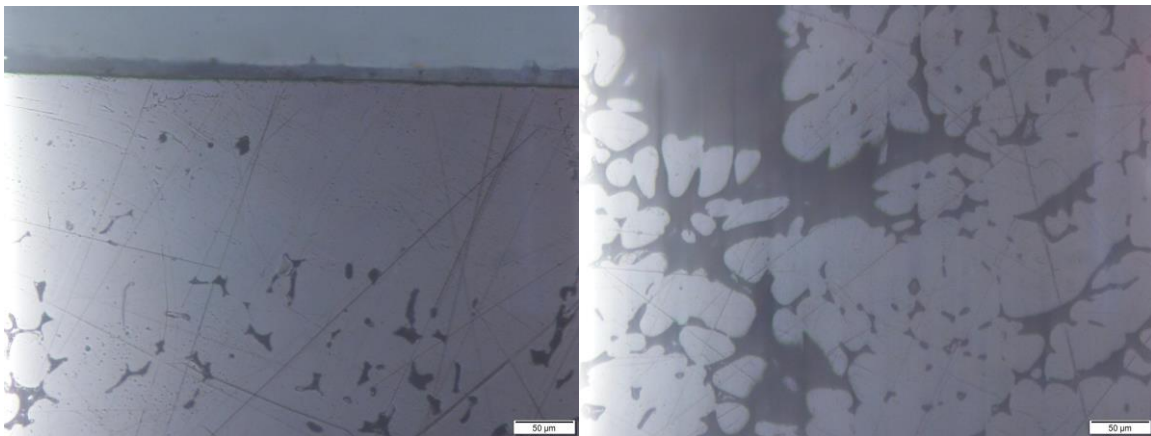


Figure 31 (Left): 20µm magnification at edge of 8 hr aged sample

Figure 32 (Right): 20µm magnification at center of 8 hr aged sample

Analysis of samples

Both samples experienced breakage at lower tensile stress and strain than expected since we expected aging to increase the strength of the rod. Optical images showed large areas of secondary phase that did not have much structure to it in the middle of the cross-section, while less secondary phase is present at the edge of the sample.

FCC+ T-phase + Laves phase (2 pieces)

The next two samples underwent heat treatment and aging to have a FCC crystal structure with both a T-phase and Laves phase present throughout. This was acquired by heat treating the samples at 480°C for 30 hours, water quenching immediately after treatment. The samples were then aged in an oven set to 300°C for 5 hours, getting water quenched immediately after as well.

Tensile testing Results

Sample Piece Five:

Load at break: 2735.547lbf

Young's Modulus: 14546.708 ksi

Tensile stress at break: 13.391 ksi

Strain % at break: 0.403

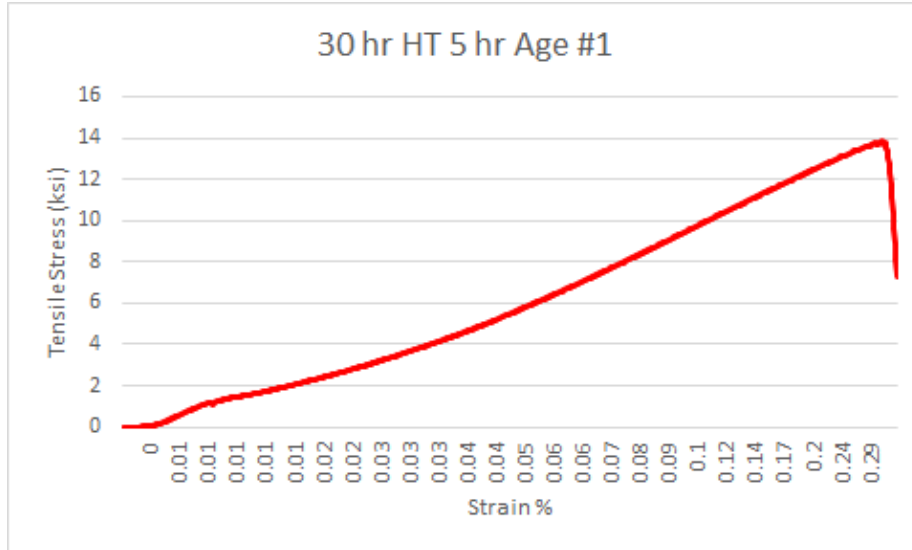


Figure 33: stress strain graph of the first 5 hr aged sample

Sample Piece Six:

Load at break: 3580.533lbf

Young's Modulus: 9564.702 ksi

Tensile stress at break: 17.527 ksi

Strain % at break: 0.284

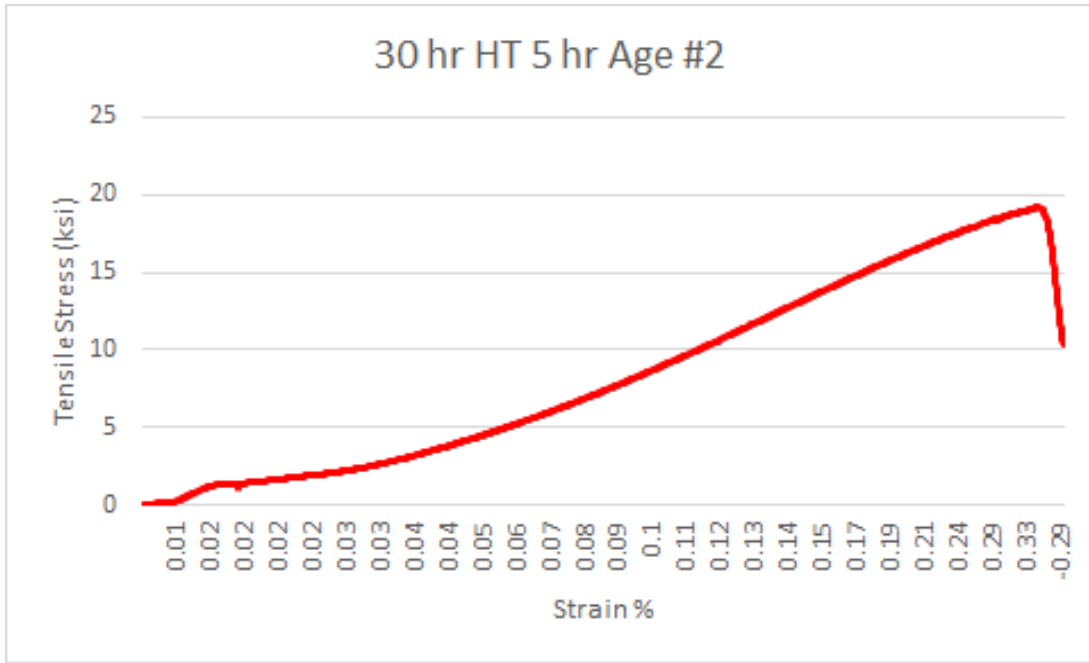


Figure 34: Stress strain graph of a second 5 hr aged sample

Optical Analysis

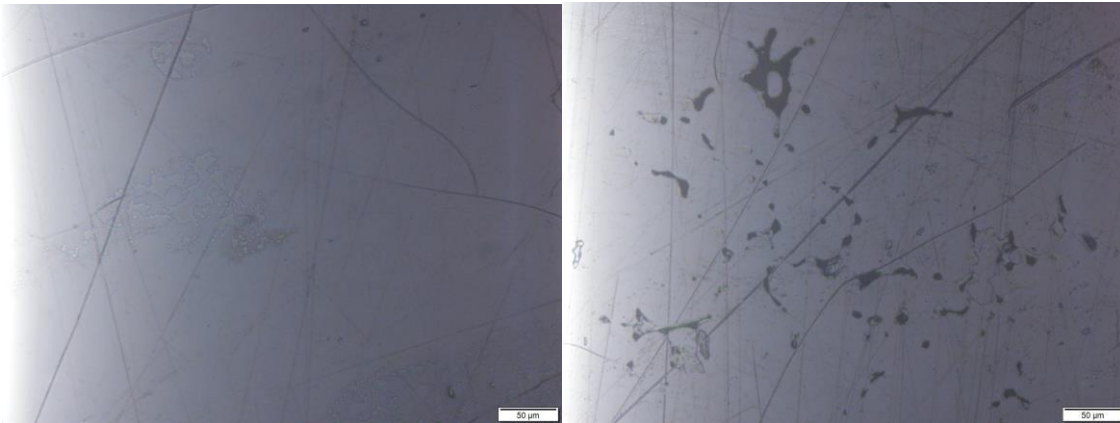


Figure 35 (Left): 20μm magnification at center of 5 hr aged sample

Figure 36 (Right): 20μm magnification at center of 5 hr aged sample

Analysis of samples

Both of the samples above broke under very low tensile stress, strain was also low. Optical analysis showed that a small amount of secondary phase was present at the middle of that sample, having some structure to it while the edge of the rod had no visible secondary phases.

As-Cast (1 piece) Tensile Testing Results

Load at break: 5616.45lbf

Young's Modulus: 11440.195 ksi

Tensile stress at break: 27.494 ksi

Strain % at break: 0.270

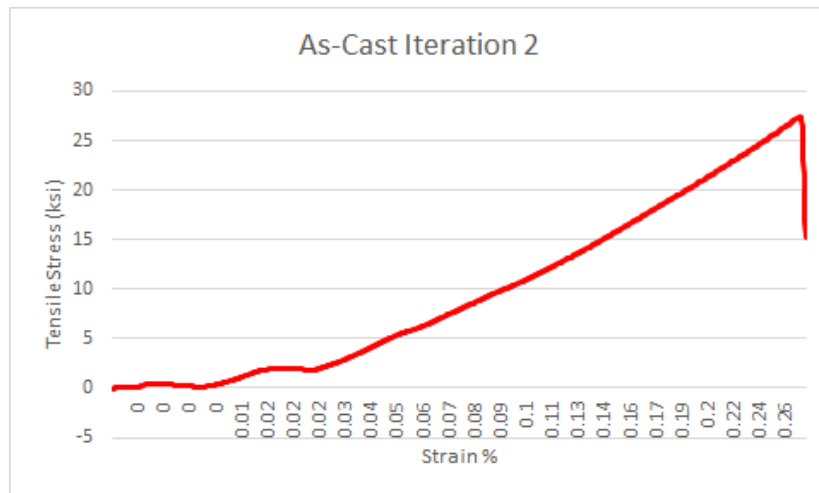


Figure 37: Stress strain graph of as cast sample

Optical Analysis:



Figure 38 (Left): Edge of sample at 20x magnification Figure 39 (Right): Middle of sample at 20x magnification

Analysis of samples

As in the previous two samples, both rods broke under low tensile stress. After looking at the optical images, we saw that the secondary phase is again present in the middle of the cross section while the edge of the sample has pour-like looking dots.

Cast One Iteration Two Conclusion

Tensile testing results:

The results were not what our team expected, but it does open a lot more questions related to this specific alloy. All samples except for the as-cast were porous throughout the breakage point, making them much weaker than the first iteration samples. There are multiple reasons this may have happened. The first is that 480°C may have caused some melting within the structure of the sample that caused it to lose strength. The second is the use of water quenching may have made the whole sample structure weaker due to the rapid cooling of the exterior and not the interior, causing unwanted aging and porosity. Even still, the as-cast was noticeably different from the results of the first iteration as-cast. This could be caused by the two week overlay between the two iterations.

1.6. Cast One Iteration Three

With the poor results found in cast one iteration two, as well as the appearance of the surface of the break, we came to the assumption that incipient melting occurred during heat treatment. What that means is that when heat treating the sample alloys at 480°C for 30 hours, some minor melting occurred around the exterior surfaces of the sample thereby making it weaker and porous once quenched. For iteration three there were 6 samples used. One as-cast, one heat treated for 30 hours at 460°C and then water quenched, two heat treated for 30 hours at 460°C water quenched then aged for 5 hours at 300°C and water quenched again. The last two were heat treated for 30 hours at 460°C, water quenched, then aged for 8 hours at 120°C, getting water quenched a second time after aging. Sadly when it came time to conduct tensile tests upon the samples, only three were able to break due to a malfunction in the tester. The three samples tested were the two 5 hour age and the 30 hour heat treat with no aging.

Pure Face Centred Cubic (FCC) (30 hr heat treatment, 0 hr aging)

Tensile Testing Results

Load at break: 9325.143 lbf

Young's Modulus: 10778.11 ksi

Tensile Stress at break: 47.303 ksi

Strain % at break: 1.193

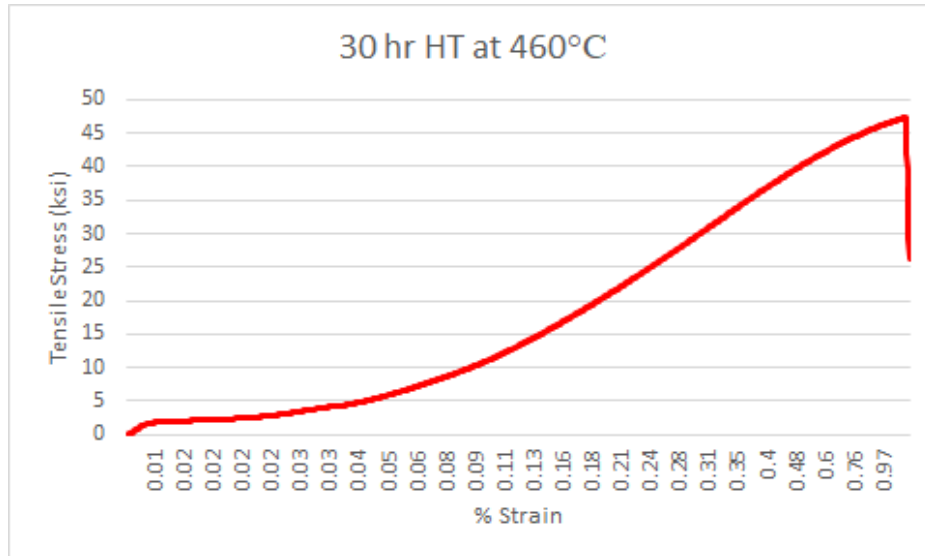


Figure 40: Stress strain graph of heat treated sample with no aging

Face Centred Cubic + T-phase + Laves phase (30 hr heat treatment, 5 hr aging)

Tensile Testing Results

Sample Piece One:

Load at break: 6202.79 lbf

Young's Modulus: 10832.904 ksi

Tensile Stress at break: 31.464 ksi

Strain % at break: 4.894

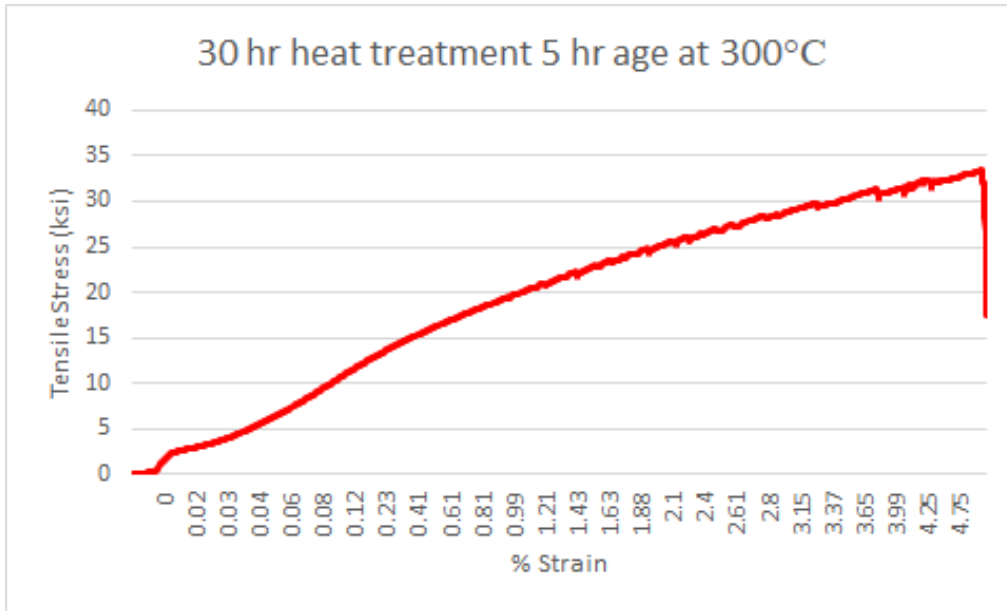


Figure 41: Stress strain graph of first 30 hr heat treated 5 hour aged sample

Sample Piece Two:

Load at break: 5116.275 lbf

Young's Modulus: 11195.667

ksi Tensile Stress at break: 25.953 ksi

Strain % at

break: 3.249

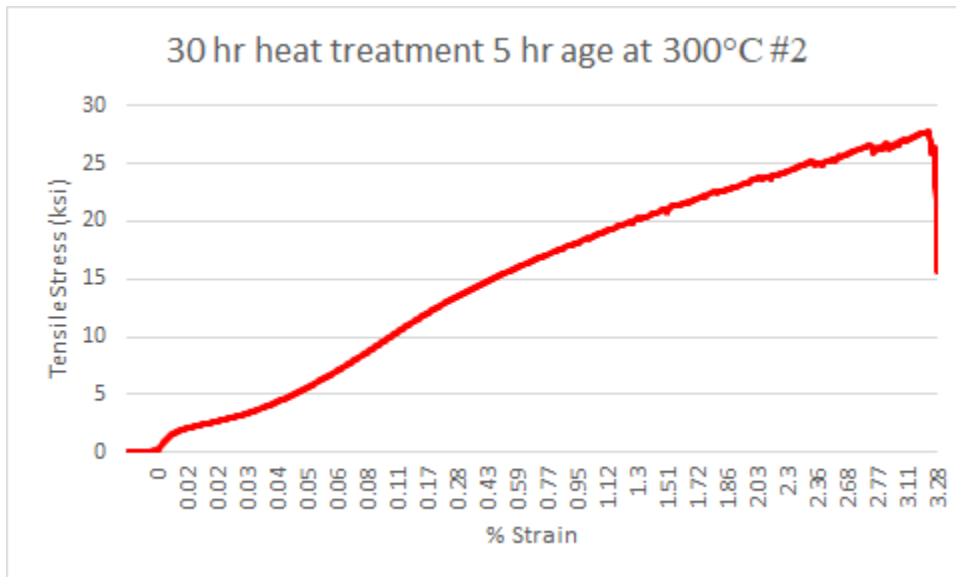


Figure 42: Stress strain graph of second 30 hr heat treated 5 hr aged sample

1.7. Final First Cast Conclusion

There were several factors that we did not take into account during our first casting process which affected our data. First, in a few cases, pouring the melt into the mold required a momentary stop in order to allow the liquid settle. This resulted in a nonuniform crystal structure that could be observed in a form of a light line on the tensile bar, which was the weakest point and often the point of breakage. Next, before casting, the mold we used was heated to a temperature of 800°F in order to allow the moderate cooling process of the liquid. We did not take into consideration that as we continued the molding process, the mold cooled down which might have resulted in weaker bonds in the tensile bars. Third, since used several different heat treatment and quenching processes on a small amount tensile bars, we were not able to draw a concrete conclusion on our testing but rather, assumptions.



Figure 43: Results of the third (left) and first (right) iteration tensile tests show the structural differences caused by melting

After tensile testing we compared the samples from iteration 2 and iteration 3. It is visible that the sample from iteration 2 is more shiny, which is attributed to the temperature difference in the aging process. The iteration 2 sample experienced melting, thus, its structure was not defined, causing a weaker bond. In all cases, heat treatment does increase Young's Modulus to some degree, although we were hoping a more significant increase.

Cast Two - Hot Tearing

2.1. Introduction

As we reviewed the results of our first cast, we found the need to study a phenomenon called hot tearing which tests the castability of a proposed alloy. Hot tearing is caused due to an uneven solidification rate of the alloy and is tested using a tree-like mold, if cracks appear on the “branches”, then hot tearing is present. Hot tearing is complex to study because it involves heat flow, fluid flow, and mass flow while several factors influence its formation; those include alloy composition, mold properties and casting design. It has been found that fine grain boundary and a controlled casting process can limit hot tearing.

For the purpose of our project, we were interested in testing the castability of an alloy which includes copper since it has high toughness as well as high electrical and thermal conductivity. It is known that the addition of copper can cause hot tearing due to its high ductility; to counteract that phenomenon, it was found that silicon can be added as it is a very brittle material. To continue our research on alloys that contain aluminum, zinc and magnesium, we decided to test how the addition of copper will affect the castability of our previously tested alloy, and how much silicon is needed to create a castable alloy. This alloy will consist of 5 elements, although the concentration of each element is too low for this to be considered a HEA, this was our first attempt of casting a complex melt such as this.

As we created the first melt, we examined the cooling curve of the melt in open air since hot tearing occurs when the melt fills the mold but doesn't solidify evenly, thus, different sections of the bar solidify at different times, causing shrinkage.[18] We found that the cooling rate is linear for the most part which indicates a consistent solidification rate throughout the melt, so our next step was to test whether hot tearing will be present.

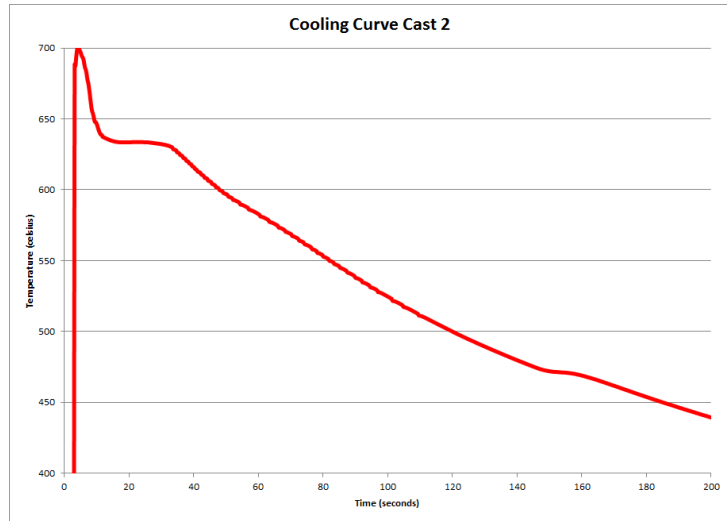


Figure 44: Cooling graph for cast 2



Figure 45: Testing the cooling rate

2.2 Hot Tearing Susceptibility

In order to analyze the hot tearing results there was a need to put them into a scientific form. Although hot tearing does not have its own unit, and it is mostly based on visual

appearance, we were able to calculate the Hot Tearing Susceptibility using a system found in a report of a research team from Syiah Kuala University, Indonesia[20]. The simple system consists of an equation and a table of reference by which we were able to rate the type of crack, the length of the rod, and the position of the crack.

There are several techniques to testing hot tearing susceptibility and those are usually classified into three different categories: tests by observation of hot tears, mechanical testing, physical property testing. For the purpose of our project, we focused on testing hot tearing by observation. This type of testing can be done using different molds such as ring mold testing, backbone mold testing, cold finger testing. The common characteristic to all those mold is the heavy end that is supposed to restrict contraction during the solidification process.[23]

Other methods that are used to measure hot tearing in a more accurate manner involve mechanical testing at high temperatures, measuring displacement during solidification, and the development of special molds that allow the direct observation of hot tears during solidification.[23]

To calculate the HTS, we took three different factors into account. First, the length of the rod (L_i) is of importance to us, if hot tearing is present, it will first occur on the longest rod since it is the weakest one, thus the longer the rod the lower its rating. Next, the width of the crack (C_i) also determines the HTS, a hairline crack is less significant than a full breakage, thus, a hairline crack will have a lower rating. Finally the location of the crack (P_i) is also a factor, a crack is most likely to take place at the sprue end of the rod rather than the ball end or the middle.

$$HTS = \Sigma(C_i \cdot L_i \cdot P_i)$$

Table 3: Hot tearing rating table

Bar Length (mm)	Li	Hot Tearing Category	Ci	Hot Tear Position	Pi
70	5	No Crack	0	Sprue End	1
120.7	4	Hairline	1	Middle Rod	3
171.5	3	Light	2	Ball End	2
222.5	2	Medium	3		
273.1	1	Complete	4		

2.2. 0% Silicon

Composition Test

Table 4: Composition of alloy before adding silicon

No	Si	Fe	Cu	Mn	Mg	Cr	Ni
	%	%	%	%	%	%	%
1	0.037	0.062	1.15	<0.0003	2.62	0.0014	0.0034
2	0.041	0.059	1.13	<0.0003	2.55	0.0021	0.0053
3	0.036	0.066	1.17	<0.0003	2.65	0.0015	0.0035
4	0.035	0.058	1.15	<0.0003	2.63	0.0015	0.0034
x	0.037	0.061	1.15	<0.0003	2.62	0.0016	0.0039

No	Ti	Ag	B	Ba	Be	Bi	Ca
	%	%	%	%	%	%	%
1	0.0004	0.0016	0.0001	<0.0001	0.0004	<0.001	0.0012
2	0.0004	0.0021	0.002	<0.0001	0.0005	<0.001	0.0015
3	0.0004	0.0016	0.0001	<0.0001	0.0005	<0.001	0.0006
4	0.0004	0.0016	0.0001	<0.0001	0.0005	<0.001	0.0012
x	0.0004	0.0017	0.0001	<0.0001	0.0005	<0.001	0.0011
No	Ce	Co	Ga	In	Li	Na	P
	%	%	%	%	%	%	%
1	<0.0015	<0.0005	0.015	0.0003	0.0001	0.0005	0.001
2	<0.0015	<0.0005	0.015	0.0003	0.0001	0.0008	0.001
3	<0.0015	<0.0005	0.015	0.0003	0.0001	0.0004	0.001
4	<0.0015	<0.0005	0.015	0.0003	0.0001	0.0006	0.001
x	<0.0015	<0.0005	0.015	0.0003	0.0001	0.0006	0.001
No	Sb	Sn	Sr	V	Zr	Hg	Al
	%	%	%	%	%	%	%
1	0.002	0.001	0.0001	0.0025	0.0003	0.002	88.9
2	0.002	0.0018	0.0001	0.0032	0.0003	0.002	89.2

3	0.002	0.001	0.0001	0.0027	0.0003	0.002	88.8
4	0.002	0.001	0.0001	0.0026	0.0003	0.002	88.9
0	0.002	0.001	0.0001	0.0027	0.0003	0.002	89

Hot Tearing Results (HTS)

Table 5: Hot tearing results for 0% silicon

Sample 1	Sample 2	Sample 3	Sample 4	Sample 5
19	19	37	19	19

*We can note that the samples are fairly consistent except for sample #3 which can be considered an anomaly. The rating for sample 3 was higher because the breakage point for two of the bars was in the middle rather than the end.



Figure 46: Hot tearing bars shortest to longest 0% silicon

We saw that the longest 4 bars have cracks in them, meaning hot tearing was present. Both the longest two bars had medium size cracks, the third bar had a light crack, while the fourth bar had a crack the size of a hairline. There was no visual crack present in the shortest bar.

2.3. 1% Silicon

Composition Test

Table 6: Composition of alloy containing 1% silicon

No	Si	Fe	Cu	Mn	Mg	Cr	Ni	Zn
	%	%	%	%	%	%	%	%
1	1.00	0.073	1.15	<0.0003	2.63	0.0008	0.003	7.01
2	1.00	0.085	1.16	<0.0003	2.62	0.0009	0.0034	7.00
3	1.00	0.0079	1.13	<0.0003	2.58	0.0008	0.0033	6.98
4	1.00	0.077	1.14	<0.0003	2.6	0.0009	0.0033	6.99
5	1.00	0.077	1.12	<0.0003	2.59	0.0009	0.003	7.02
x	1.00	0.078	1.14	<0.0003	2.6	0.0009	0.0032	7.00
No	Ti	Ag	B	Ba	Be	Bi	Ca	Cd
	%	%	%	%	%	%	%	%
1	0.0004	0.0016	0.0006	<0.0001	0.0004	<0.001	0.0016	0.0001
2	0.0004	0.0016	0.0007	<0.0001	0.0005	<0.001	0.0018	0.0001
3	0.0004	0.0017	0.0005	<0.0001	0.0004	<0.001	0.0018	0.0001
4	0.0004	0.0016	0.0007	<0.0001	0.0004	<0.001	0.004	0.0001

5	0.0004	0.0016	0.0007	<0.0001	0.0004	<0.001	0.0038	0.0001
x	0.0004	0.0016	0.0006	<0.0001	0.0004	<0.001	0.0026	0.0001
No	Ce	Co	Ga	In	Li	Na	P	Pb
	%	%	%	%	%	%	%	%
1	<0.0015	<0.0005	0.015	0.0003	0.0001	0.0002	0.001	0.0005
2	<0.0015	<0.0005	0.015	0.0003	0.0001	0.0001	0.001	0.0005
3	<0.0015	<0.0005	0.015	0.0003	0.0001	0.0002	0.001	0.0005
4	<0.0015	<0.0005	0.015	0.0003	0.0001	0.0002	0.001	0.0005
5	<0.0015	<0.0005	0.015	0.0003	0.0001	0.0003	0.001	0.0005
x	<0.0015	<0.0005	0.015	0.0003	0.0001	0.0002	0.001	0.0005
No	Sb	Sn	Sr	V	Zr	Hg	Al	
	%	%	%	%	%	%	%	
1	0.002	0.001	0.0001	0.0027	0.0003	0.002	88.1	
2	0.002	0.001	0.0001	0.0028	0.0003	0.002	88.1	
3	0.002	0.001	0.0001	0.0036	0.018	0.002	88.2	
4	0.002	0.001	0.0001	0.0034	0.027	0.002	88.1	
5	0.002	0.001	0.0001	0.0025	0.0003	0.002	88.2	
x	0.002	0.001	0.0001	0.003	0.0081	0.002	88.1	

Hot Tearing Results (HTS)

Table 7: Hot tearing results for 1% silicon

Sample 1	Sample 2	Sample 3
13	13	13



Figure 47: Hot tearing sample bars shortest to longest for 1% silicon

All the 1% silicon samples had defects in the longest 3 bars. In the sample presented above, the longest bar was not properly casted because the melt was not poured fast enough, we considered the longest bar to have crack the size of the other cracks present in the other two 1% silicon samples, a medium size. The second largest bar had a light crack while the third shortest bar had a hairline crack. The shortest two bars did not have visual cracks.

2.4. 3% Silicon

Composition Test

Table 8: Composition of alloy containing 3% silicon

No	Si	Fe	Cu	Mn	Mg	Cr	Ni	Zn
	%	%	%	%	%	%	%	%
1	3.05	0.131	1.12	<0.0003	2.57	0.0009	0.0031	7.02
2	3.13	0.127	1.13	<0.0003	2.6	0.0008	0.003	7.01
3	3.02	0.113	1.11	<0.0003	2.53	0.0008	0.0028	6.92
4	3.05	0.118	1.13	<0.0003	2.55	0.0008	0.0028	7.06
5	3.03	0.127	1.11	<0.0003	2.59	0.0008	0.0028	7.03
x	3.06	0.123	1.12	<0.0003	2.57	0.0008	0.0029	7.01
No	Ti	Ag	B	Ba	Be	Bi	Ca	Cd
	%	%	%	%	%	%	%	%
1	0.0004	0.0016	0.0008	<0.0001	0.0004	<0.001	0.0037	0.0001
2	0.0004	0.0016	0.0013	<0.0001	0.0005	<0.001	0.0031	0.0001
3	0.0004	0.0016	0.0009	<0.0001	0.0004	<0.001	0.0016	0.0001
4	0.0004	0.0016	0.001	<0.0001	0.0004	<0.001	0.0014	0.0001
5	0.0004	0.0016	0.0006	<0.0001	0.0004	<0.001	0.0028	0.0001

x	0.0004	0.0016	0.0009	<0.0001	0.0004	<0.001	0.0025	0.0001
No	Ce	Co	Ga	In	Li	Na	P	Pb
	%	%	%	%	%	%	%	%
1	<0.0015	<0.0005	0.014	0.0003	0.0001	0.001	0.001	0.0005
2	<0.0015	<0.0005	0.014	0.0003	0.0001	0.0008	0.001	0.0005
3	<0.0015	<0.0005	0.015	0.0003	0.0001	0.0002	0.001	0.0005
4	<0.0015	<0.0005	0.015	0.0003	0.0001	0.0003	0.001	0.0005
5	<0.0015	<0.0005	0.014	0.0003	0.0001	0.0007	0.001	0.0005
x	<0.0015	<0.0005	0.014	0.0003	0.0001	0.0006	0.001	0.0005
No	Sb	Sn	Sr	V	Zr	Hg	Al	
1	0.002	0.001	0.0001	0.0033	0.0003	0.002	86.1	
2	0.002	0.001	0.0001	0.0031	0.0003	0.002	86	
3	0.002	0.001	0.0001	0.0031	0.0003	0.002	86.3	
4	0.002	0.001	0.0001	0.0033	0.011	0.002	86	
5	0.002	0.001	0.0001	0.0031	0.0003	0.002	86.1	
x	0.002	0.001	0.0001	0.0032	0.0013	0.002	86.1	

Hot Tearing Results (HTS)

Table 9: Hot tearing results for 3% silicon

Sample 1	Sample 2	Sample 3
0	0	0



Figure 48: Hot tearing sample for 3% silicon

In the 3% silicon, there were no visual cracks present in any of the bars, meaning no hot tearing was present.

2.5. Final Second Cast Conclusion

Looking at the hot tearing results presented above, we saw that the addition of silicon significantly improved the castability of the melt. When 1 weight percent silicon was added, hairline cracks were still present in the longest 2-3 bars, thus, there was a need to add more silicon. The cast containing 3 weight percent silicon did not have cracks in any of the bars, meaning there was no visible hot tearing. For future casts, we can conclude that it is necessary to add silicon when copper is present in order to create a castable melt.

Final Conclusion

Throughout the span of the project, multiple methods and practices were used to draw up conclusions related to the alloys we created along with future iterations involving certain elements. These conclusions were based on the use of computer modelling and its accuracy to the results found during experimentation. From this and extensive error analysis, we were able to provide the following conclusions.

In the first cast, we used multiple ICME programs to determine the projected phases of the alloy. From these diagrams, we were able to create a proper heat treatment schedule with the correct temperatures to achieve the desired phase. By looking at our results in the first and second iteration, we found that the temperature was too high in the second and provoked incipient melting in multiple samples, making those samples have poor mechanical properties. By the third iteration the proper heat treatment and aging temperatures were found and implemented and created samples with improved mechanical properties when compared to the as-cast.

As for the second cast, we again used ICME programs to create another alloy, this time using aluminum, magnesium, zinc, and now copper. The purpose of this cast was to see the improvements in castability of the alloy when percentages of silicon were added incrementally. Three tests were conducted, one at 0wt% silicon, one at 1wt% and one at 3wt% silicon. From these tests, it was proved that the addition of silicon greatly improved the castability of the alloy, going from a HTS score of 19 to a score of 0.

The data found in this project was an important step in the finding and creation of a new high entropy aluminum alloy. With the help of alloy modelling via ICME programs, we were able to save time and resources by drawing basic mechanical property assumptions of certain alloys instead of doing many casts of alloys with minute composition differences. By testing a ternary alloy and finding solutions to all errors, we were able to move on to a quaternary system and make conclusions on that as well as the quinary system we constructed at the end involving aluminum, magnesium, zinc, copper, and silicon. With the conclusions we proved and the error analysis conducted, we can now continue with further mechanical testing and heat treatment of

the alloys made in the second cast in order to create a new high entropy alloy with superior mechanical properties over other existing alloys.

References

- [1] D. Miracle and O. Senkov, “A critical review of high entropy alloys and related concepts,” *Acta Materialia*, vol. 122, pp. 448–511, Jan. 2017.
- [2] I. S. Aristeidakis and M. I. T. Tzini, “High Entropy Alloys,” *High Entropy Alloys*, Jan-2016. [Online]. Available: http://www.mie.uth.gr/ekp_yliko/HighEntropyAlloys.pdf. [Accessed: 25-Jul-2018].
- [3] C. Koch and M. Shipman, “New 'High-Entropy' Alloy Is As Light As Aluminum, As Strong as Titanium Alloys,” *NC State News*, 10-Dec-2014. [Online]. Available: <https://news.ncsu.edu/2014/12/koch-high-entropy-alloy-2014/>. [Accessed: 25-Jul-2018].
- [4] S. Qiu, N. Miao, J. Zhou, Z. Guo, and Z. Sun, “Strengthening mechanism of aluminum on elastic properties of NbVTiZr high-entropy alloys,” *Intermetallics*, vol. 92, pp. 7–14, Jan. 2018.
- [5] S. Wang, *Figure 5*. MDPI, 2013.
- [6] D. B. Miracle, “High-Entropy Alloys: A Current Evaluation of Founding Ideas and Core Effects and Exploring ‘Nonlinear Alloys,’” *Jom*, vol. 69, no. 11, pp. 2130–2136, Nov. 2017.
- [7] “Primary Metallic Crystalline Structures,” *Conductors and Insulators*. [Online]. Available: https://www.nde-ed.org/EducationResources/CommunityCollege/Materials/Structure/metallic_structures.htm. [Accessed: 25-Jul-2018].
- [8] “FCC, BCC and HCP Metals.” [Online]. Available: <http://che.uri.edu/course/che333/Structure.pdf>. [Accessed: 25-Jul-2018].
- [9] A. Scrimshire, *Lattice structures of FCC, BCC and HCP structures*
- [10] G. Darja, “High-entropy Alloys,” *High-entropy Alloys*, Jan-2017. [Online]. Available: http://mafija.fmf.uni-lj.si/seminar/files/2016_2017/High-entropy_alloys.pdf. [Accessed: 25-Jul-2018]
- [11] S. Wang and Y. Liu, *Figure 1*. ScienceDirect, 2018.
- [12] J. R. Davis, “Aluminum and Aluminum Alloys,” *Alloying: Understanding the Basics*, pp. 351–416, 2001.
- [13] J. Allison, D. Backman, and L. Christodoulou, “Integrated computational materials engineering: A new paradigm for the global materials profession,” *Jom*, vol. 58, no. 11, pp. 25–27, 2006.
- [14] U. R. Kattner, “The Calphad Method And Its Role In Material And Process Development,” *Tecnologia em Metalurgia Materiais e Mineração*, vol. 13, no. 1, pp. 3–15, 2016.
- [15] D. Naujoks and A. Ludwig, *Graphical abstract of a CALPHAD phase diagram*. ScienceDirect, 2017.

- [16] D. Diez, "Metallography – an Introduction," *Leica Microsystems*, 18-Oct-2013. [Online]. Available: <https://www.leica-microsystems.com/science-lab/metallography-an-introduction/>. [Accessed: 25-Jul-2018].
- [17] Li, S., and D. Apelian. *HOT TEARING OF ALUMINUM ALLOYS A CRITICAL LITERATURE REVIEW*. American Foundry Society, 2011, *HOT TEARING OF ALUMINUM ALLOYS A CRITICAL LITERATURE REVIEW*.
- [18] "Hot Tearing." *United Precious Metal Refining, Inc.*, www.unitedpmr.com/hot_tearing.php.
- [19] Brûna, Marek. "Hot Tearing Evaluation for Aluminium Alloys." *AIP Publishing*, American Institute of Physics, 30 June 2016, aip.scitation.org/doi/abs/10.1063/1.4953697?journalCode=apc.
- [20] Akhyar, H., & Malau, V. (2017, February 28). Hot tearing susceptibility of aluminum alloys using CRCM-Horizontal mold. Retrieved August 5, 2018, from <https://www.sciencedirect.com/science/article/pii/S2211379717303285>
- [21] Cui, Wenyuan, et al. *Additive Manufacturing of High Entropy Alloys*. The 28th Annual International Solid Freeform Fabrication Symposium, 2017, *Additive Manufacturing of High Entropy Alloys*.
- [22] Yeh, J., & Davison, A. (2006). *High-entropy alloys / Alliages a haute entropie / coordonnateurs*, Jien-Wei Yeh, Andrew Davison. Cachan: Lavoisier.
- [23] Li, S. (2010). Hot Tearing in Cast Aluminum Alloys: Measures and Effects of Process Variables (Doctoral dissertation, Worcester Polytechnic Institute) [Abstract]. 23-31.

Appendix A: Modelling Process

The ternary phase diagrams (see figures 5-8) were created using Pandat to calculate the phases of aluminum, zinc and magnesium alloys at 250°C, 350°C, 450°C and 550°C. These diagrams were used to determine the heat treatment temperature and composition of the alloy required to produce pure FCC. The diagram in Figure 9 was created using Thermo-Calc to calculate the mole fraction of magnesium, which at a 450°C heat treatment, would produce a pure FCC structure. Figure 10 was created using Thermo-Calc to calculate the phase fraction of the alloy at various temperatures.

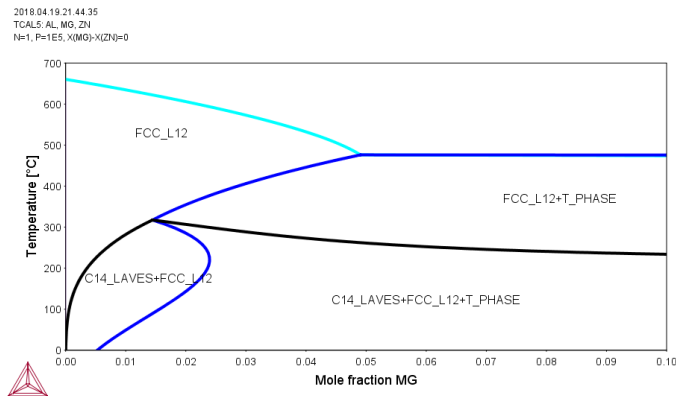


Figure 49: Diagram created using Thermo-Calc

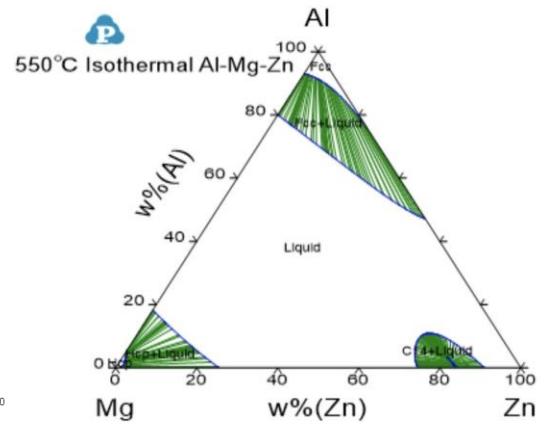


Figure 50 : Diagram created using Pandat

Appendix B: Casting Process

When casting each alloy, this general guideline was used to melt, add, and mix the molten material. The first step in casting is to make sure the foundry is clean and ready to use, including the oven, mold, and any necessary ladles. Once this is all set, we turned the oven on and let it get to 800 degrees fahrenheit with the desired mold inside of it.

We then calculated how much of each metal we need. We do this by taking the desired atomic percent and calculating it into weight percent using the following formulas.

$$\sum_n^0 p * at\% = p_{total} \qquad \frac{\rho * at\%}{p_{total}} = w \qquad \frac{w}{100} = wt\%$$

We then figure out the total mass of the melt needed to make the necessary amount of sample pieces. From this we can use the weight percent and the total mass to find out the mass of each metal necessary to create our alloy.

$$total\ mass\ of\ melt * wt\% = desired\ mass\ of\ element$$

Once the mass of each element is determined, we then go to the ingot room in Washburn to collect the raw materials. We then find all of the elements we need and cut and weigh them until we have the right amount. From this we can go into the foundry and begin to melt the materials.

Melting

Being an aluminum based alloy, we begin by melting the aluminum. We place the aluminum block into the induction furnace and turn it on. We turn the knob between 30 and 35, which is about 20 kilowatts of power. We place insulation around the opening to preserve heat and speed up melting.



Figure 51 (Left): Induction furnace control Panel

Figure 52 (Right): Induction furnace with aluminum block

After the material is fully melted, we then added the other metals one by one, making sure that they fully melt before adding more. Once the melt has all elements present and fully melted, we then heat up a ladle over the melt and take one scoop and put it into the testing mold. We let the mold cool and then bring the sample upstairs to test its material properties.



Figure 53 (Left): Adding metals to melted aluminum

Figure 54 (Right): Preparing sample for composition tester using belt sander

Testing Material Properties

Once upstairs we tested the material properties of the sample via an alloy composition tester. This machine gave us an accurate weight percentage of each element. After testing five times on different sections of the sample, we got an average of each element. We compared this number to our desired weight percent and if too far off the desired number, we would add that material into the melt and recast another sample piece and check the weight percent again. We would repeat this until our desired weight percentages were met.



Figure 55 (Left): Composition testing sample

Figure 56 (Right): Bottom of sample after numerous composition tests

Degassing (Cast One Only)

Once we know we have our desired alloy present, we then gassed the melt. This involves us putting in a rotating tube with argon gas coming out of small holes present in the tube. This removes any bubbles and air from the mold so it does not oxidize. We left this for 15 minutes. After the allotted time, we then began to cast sample pieces.

Casting into mold (Cast One)

Once degassed, the first cast was ready to be poured into the tensile test mold. The mold was in an 800°F oven for the day so when we took it out it was 800°F as well. Once the mold was out, we took the larger ladle and filled it with the melt. We then quickly poured the melt into the mold, making sure it did not overflow or miss the opening. After letting the molten alloy cool in the mold, we then opened the mold and took out the tensile test bars. This process was repeated until all melt was used.

Casting into mold (Cast Two)

In cast two, the alloy was not degassed, therefore once fully melted and the desired composition was met, it was ready to pour. The mold was temperature controlled using a hot plate. Above the mold was a gritty sand cone that functioned as a funnel for the melt to go into the mold. Once the mold reached a temperature of 305°C and the melt at a temperature of 755°C it was ready to pour. A full large ladle was taken from the melt and quickly poured into the mold. It then sat for a couple minutes to cool, then the mold was opened and the castability samples were taken out.

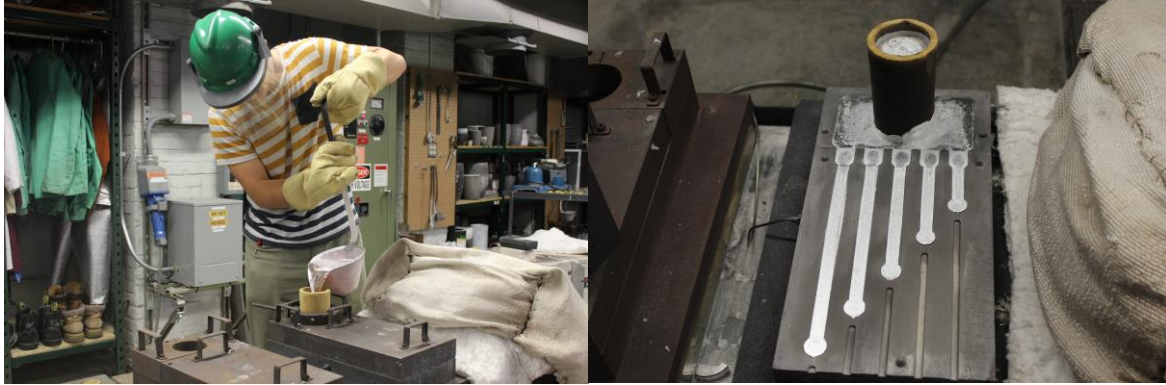


Figure 57 (Left): Melt being poured into castability mold

Figure 58 (Right): Cooled alloy in mold ready to be removed

Appendix C: Tensile Testing

When tensile testing each sample of the alloy, this general guideline was followed to properly and safely find the mechanical properties of each piece.

Safety

Proper safety gear is necessary in order to not harm oneself when operating machinery whose objective is to break an object. Safety glasses are required when tensile testing so that no shrapnel from the break end up in your eyes. Gloves are not recommended because they could get stuck in the tensile testing clamps.

Startup and Loading Piece

For this project, we used an Instron Tensile tester hooked up to one to the lab computers. The first step is to turn on the tensile tester and let it warm up before opening the application on the computer, otherwise the machine would not register. Once the machine and application have successfully loaded and paired, the sample pieces are ready to load.



Figure 59 (Left): Untested sample

Figure 60 (Right): Tensile testing machine controls

When loading samples into the tester, the correct grips must be installed. For this project we used cylindrical test pieces, so the curved grips were used in the tester. If the square grips were on the machine, we simply changed them out to the curved grips using a conventional allen wrench. With the correct grips installed, put the machine into HIGH gear. This allows it to jog up and down faster for loading. Loosen the top grip, load the sample piece, and tighten the clamps onto the sample. Now jog the grip down, making sure the sample piece goes into the lower grips.

Once lowered far enough, tighten down the lower grips onto the sample piece. With the sample ready for testing, switch the tester into LOW gear for testing. Once fully loaded, apply the strain sensor onto the breakage region of the sample piece, making sure to zero it once properly installed to the sample. Now that everything is ready, start the program and wait for the sample to break. Once broken, identify if the piece broke within the specified region to see if the data would be valid.



Figure 61 (Left): Sample in tensile testing machine

Figure 62 (Right): Sample after testing

Appendix D: Polishing Process

After each sample has been mechanically tested using the tensile test machine, it is then put through the polishing process to allow us to observe each sample under the microscope and SEM machine. This process is required because with such intense polishing it removed all scratches on the metals surface to allow us to strictly observe the grains and grain boundaries without any visual obstructions. The process includes cutting, resin molding, and finally polishing.

Before Starting

Before beginning the polishing process, we had to go through a checklist of safety and operation checks. This involved making sure all members were wearing correct attire and had safety glasses. Then we checked if the saw had enough coolant in the chamber, and if not filled it with the correct coolant. The next is turning on the water and compressed air for the polisher and resin compressor. Without these on the machines would not function properly and might damage the machines. The final item checked was how full the polishing waste container was. If it was close to full, it was replaced with a new container and the lab coordinator was notified.

Cutting

The first step in the polishing process is cutting. This is required because the tensile testing cast is too large and only a $\frac{1}{4}$ inch of the sample is needed. Before the cutting begins we put in then appropriate blade speed, cut rate, and blade travel distance into the Buehler precision saw. The sample is loaded in the saw and is automatically cut. This process is repeated for each sample. The cut makes a smooth surface on one end of the sample, which is necessary for polishing.



Figure 63: Buehler metal cutter used in project

Resin Molding

The next step in the polishing process is putting the cut sample into a Buehler molding compressor. This puts the sample with a mixture of resin powder under high temperature and pressure in order for the resin to mold around the sample to allow the sample to fit within the polisher. We began by applying a non binding powder to the top of the piston and on the cap. We then put the sample smooth side down onto the piston and lower it into the chamber. After it is at the bottom. We pour one scoop of resin powder into the chamber. This can compress up to two samples. If a second sample is to be compressed, a powdered second plate is placed above the resin powder with another sample on top. The two are then lowered into the chamber and a second scoop of resin is put in for the top sample. The cap is then put on and locked. The resin binds at a certain pressure, temperature, and time. So we apply those settings into the machine and press start. After the compression process is completed, the sample is ejected from the chamber. We then use a Dremel to carve in the sample information into the resin such as sample number and heat treatment time.



Figure 64: Buehler resin sample moulder used in project

Polishing

The final machine used in the polishing process is the Buehler polisher. Each sample is loaded into a ten spot tray. If there were less than ten samples, spacers are put into the empty spots in order for each sample to be tightened into place. This is loaded into the polisher head and turned and locked into place. On the screen we adjusted the force based on the number of samples and made sure the selected force was central due to the tray we were using. With an aluminum heavy sample, we used Buehler's standard aluminum polishing five step procedure. The steps include 350 grit sandpaper, 5 μ m, 3 μ m, 1 μ m, and lastly a silica based lubricant. For each step the specific pad was put onto the platen and was covered in the specific lubricant before starting the step, making sure to use the correct lubricant in order to not contaminate the pad. After the pad was well lubricated, the sanding process was initiated. The samples would be lowered onto the spinning platen, with the tray either spinning with or against the rotation of the platen, for the allotted time. After each step, the samples would get cleaned with water and dried with an air gun. They would then be observed to see if there are any major scratches or imperfections which may lead to the repeating of steps.



Figure 65: Buehler polisher used in project

Appendix E: Optical Analysis Process

After the polishing of the first iteration, each of the four samples were analysed under a high magnification Nikon microscope. Here we got an idea of how the added metals were dispersed throughout the different heat treated samples. We focused on the difference between present precipitations both at the edge and at the center.



Figure 66 (Left): Polished sample and carrying vessels

Figure 67 (Right): Nikon Microscope with sample being analysed